Table 2. *Biochemical analysis of BALF*

	TP, μg/ml	IgE, ng/ml	IL-4, pg/ml	IL-5, pg/ml	IFN-γ, pg/ml	LT C4/D4/E4, pg/ml
$AM^{+/+}$ Saline (n = 5)	4.94±1.91	5.30±0.85	1,092.3±17.1	17.0±3.8	1,492.4±129.0	25.3±1.3
$AM^{+/-}$ Saline (n = 5)	4.82±0.54	4.44±0.92	834.1±28.2	10.2±1.2	1,548.4±119.2	4.3±0.5
$AM^{+/+}$ OVA (n = 9)	40.20±18.22	70.58±15.00	938.9±28.7	41.8±14.6	1,353.0±66.6	41.4±26.4
$AM^{+/-}$ OVA (n = 7)	21.13±8.75	60.02±12.41	759.3±23.0	23.9±7.1	1,624.3±119.2	15.6±4.8

Values are means ± SE. TP, total protein; IgE, immunoglobulin E; IL-4, interleukin-4; IL-5, interleukin-5; IFN-γ, interferon-γ; LT C4/D4/E4, leukotriene C4/D4/E4.

same conditions other than the usage of mouse IgG2a negative control (DAKO Cytomation, catalog no. X0943) instead of anti-α-SM actin antibody at the same immunoglobulin concentration.

Materials and chemicals. Materials and chemicals were obtained from Sigma Chemical (St. Louis, MO) unless otherwise specified.

Data analysis. Comparisons of data among the experimental groups were carried out with one-way ANOVA (Scheffe's test) or the nonparametric Kruskal-Wallis test. Statistical significance was determined by P values under 0.05, and errors are given in SE (standard error) unless otherwise stated. The program Microsoft Excel 2003 was used for data management, and all statistics were performed using SPSS II (SPSS Japan, version 14.0).

RESULTS

Airway responsiveness to MCh administration. There were no significant differences in baseline RL and lung elastance among each group. MCh dose response curves for RL are demonstrated in Fig. 1. $AM^{+/-}$ mice showed the elevation of RL to MCh dose of 2.5–5 mg/ml, whereas the other groups exhibited no significant responses.

Airway responsiveness was also assessed using $EC_{200}R_L$ (Fig. 2: saline-treated $AM^{+/+}$, 16.81 ± 2.01 mg/ml; saline-treated $AM^{+/-}$, 16.73 ± 2.34 mg/ml; OVA-treated $AM^{+/+}$, 7.95 ± 0.98* mg/ml; OVA-treated $AM^{+/-}$, 2.41 ± 0.63 mg/ml, respectively; *$P < 0.05$ vs. the other groups). Although bronchial hyperresponsiveness to MCh was observed in the OVA-challenged wild-type mice, responses in the OVA-challenged $AM^{+/-}$ mice were significantly enhanced compared with the OVA-treated wild-type mice.

Assessment of the BALF. Cell fractions in BALF are shown in Table 1, indicating the increases in the eosinophil fractions in the OVA-sensitized groups. No differences in the fraction and the number of BALF eosinophil were observed between the OVA-treated wild-type and the mutant mice. Measurements of total IgE levels [saline-treated $AM^{+/+}$, 5.30 ± 0.85 ng/ml (n = 5); saline-treated $AM^{+/-}$, 4.44 ± 0.92 ng/ml (n = 5); OVA-treated $AM^{+/+}$, 4.19 ± 2.33 ng/ml (n = 9); OVA-treated $AM^{+/-}$, 4.40 ± 1.69 ng/ml (n = 7), respectively] showed no significant differences among each group. Total protein amount in BALF was also assessed [saline-treated $AM^{+/+}$, 45.05 ± 12.40 μg/ml (n = 6); saline-treated $AM^{+/-}$, 43.35 ± 7.00 μg/ml (n = 5); OVA-treated $AM^{+/+}$, 82.47 ± 23.60 μg/ml (n = 9); OVA-treated $AM^{+/-}$, 69.64 ± 14.70 μg/ml (n = 7), respectively], but no differences were found among each group. IL-4, 5, IL-13, and IFN-γ were measured, but no difference was found between OVA-treated mutant mice and OVA-treated wild-type mice. The level of LTC4/D4/E4 in BALF obtained from each group was also measured, but no differences were found either (Table 2).

Table 3. *Immunoreactivity analysis of serum*

	OVA-specific IgG1, U/ml	OVA-Specific IgE, U/ml
$AM^{+/+}$ Saline	ND	ND
$AM^{+/-}$ Saline	ND	ND
$AM^{+/+}$ OVA (n = 6)	5,578.4±4,513.1	ND
$AM^{+/-}$ OVA (n = 7)	1,879.6±1,389.3	ND

Values are means ± SE. ND, not detected.

Assessment of the serum. Antigen exposure increased the OVA-specific IgG1 levels [OVA-treated wild-type mice, 5,578.40 ± 4,513.11 U/ml (n = 7); OVA-treated mutant mice, 1,879.62 ± 1,389.27 U/ml (n = 7); saline groups not detectable], whereas no difference was observed between OVA-treated mutant mice and OVA-treated wild-type mice. Meanwhile, the OVA-specific IgE in serum was not detectable (Table 3).

ir-ADM. ir-ADM levels in the lung tissue were demonstrated in Fig. 3. ir-ADM levels of OVA-treated groups did not significantly differ from those of OVA-untreated groups. ir-ADM levels of the mutant groups before MCh challenge were also lower than those of the wild-type groups. MCh inhalation enhanced these immunoreactivities of each group ($P < 0.01$). ir-ADM levels after MCh inhalation were significantly different between OVA-untreated wild-type mice and OVA-untreated mutant mice ($P < 0.01$). Similarly, ir-ADM level of the OVA-treated mutant mice after MCh challenge was lower than that of the OVA-treated wild-type mice ($P < 0.01$).

Semi-quantitative assessment of eosinophilia and airway hypersecretion. As shown in Fig. 4, mononuclear cells or eosinophils infiltrated markedly along the airways of the OVA-treated mice, whereas no difference was found between the wild-type and the mutant mice. On the Luna-stained tissue, eosinophils were markedly found around the airways of the OVA-challenged groups, but the degree of eosinofil infiltration showed no significant difference between the $AM^{+/+}$ and the

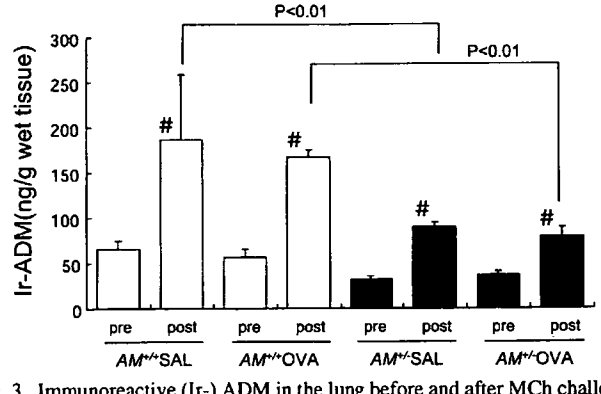

Fig. 3. Immunoreactive (Ir-) ADM in the lung before and after MCh challenge (RIA). $P < 0.01$ compared with the postinhalation value of $AM^{+/+}$ OVA group. #$P < 0.01$ compared with the preinhalation value.

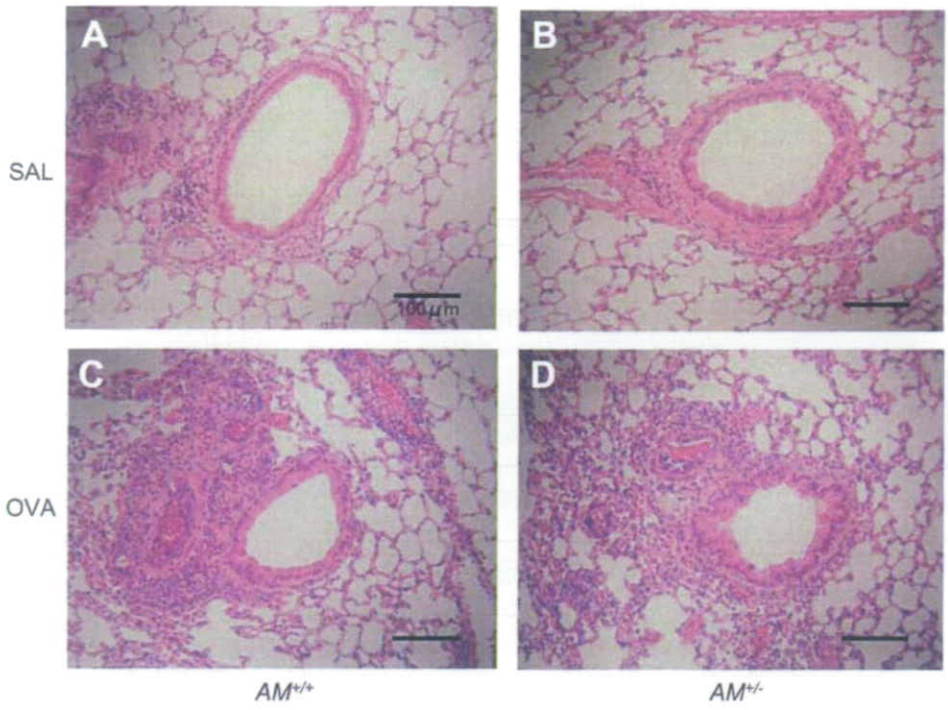

Fig. 4. Photomicrographs of small airways and lung parenchyma from saline-treated wild-type (*A*), saline-treated ADM mutant (*B*), OVA-treated wild-type (*C*), or OVA-treated ADM mutant mice (*D*). Specimens were stained with hematoxylin and eosin. Scale bar, 100 μm.

$AM^{+/-}$ mice (Fig. 5). OVA-treated groups apparently showed very intense staining of PAS/Alcian blue, suggesting goblet cell hyperplasia and airway mucus hypersecretion. Although the OVA challenge caused the significant change in both animal groups, the magnitude of goblet cell hyperplasia and airway mucus hypersecretion was not different between the wild-type mice and the mutant mice (Fig. 6).

Morphometric analysis. Ai/Abm of the OVA-treated mutant mice was significantly smaller than that of the OVA-untreated mutant type mice ($P = 0.0007$), but it was not different from that of the OVA-treated wild-type mice ($P = 0.20$) (Fig. 7). Ae/Abm of the OVA-treated mutant mice was greater than that of the OVA-untreated mutant mice ($P = 0.00007$), but it was not different from that of the OVA-treated wild-type mice ($P = 0.20$) (Fig. 8). Similarly, Asm/Abm of the OVA-treated mutant mice was also larger than that of the OVA-untreated mutant mice ($P = 0.00007$). However, Asm/Abm of the OVA-treated mutant mice was significantly greater than that of the OVA-treated wild-type mice ($P = 0.00010$) (Fig. 9). The number of cells in the airway smooth muscle layer of the OVA-treated mutant mice was significantly greater than that of the OVA-untreated mutant mice ($P = 0.0019$) or that of the OVA-treated wild-type mice ($P = 0.012$) (Fig. 10).

Assessment of airway smooth muscle mass of the tissue sections immunohistochemically stained with α-SM actin antibody (Fig. 11) was also performed. Asm/Abm of the OVA-treated mutant mice was significantly greater than that of the OVA-treated wild-type mice ($P = 0.0004$) (Fig. 12).

DISCUSSION

The current study clearly revealed greater AHR of the heterozygous ADM mutant mice in the allergen-induced asthma model. To our knowledge, this is the first report to study whether ADM gene function could be involved in the AHR using mutant mice. In addition, the MCh dose, which causes significant elevation of R_L in $AM^{+/-}$ mice, was very lower than that of the usual model of AHR in other mice. Thus the enhanced AHR suggests that innate ADM might play a pivotal role in AHR in allergen-induced asthma.

We observed that ir-ADM level after MCh challenge was significantly greater in the wild than in the mutant. This finding

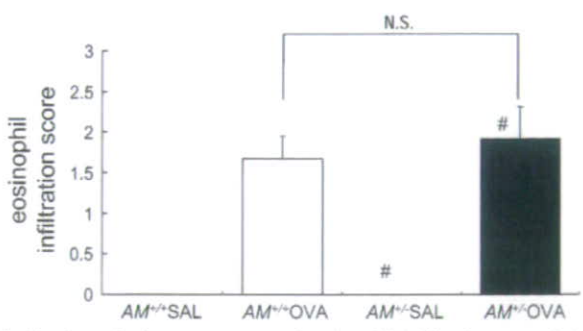

Fig. 5. Semi-qantitative assessment of eosinophil infiltration around the airways. #$P < 0.05$ compared with the saline group in the same strain.

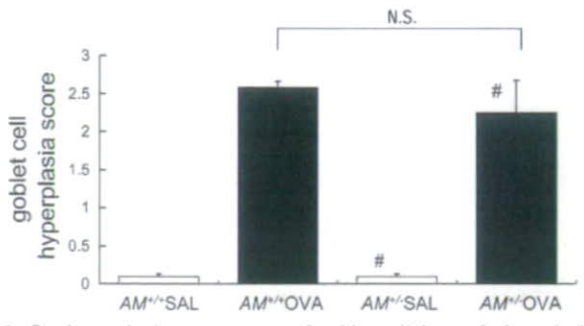

Fig. 6. Semi-quantitative assessment of goblet cell hyperplasia and airway hypersecretion of wild-type and mutant mice with OVA inhalation challenge. #$P < 0.05$ compared with the saline group.

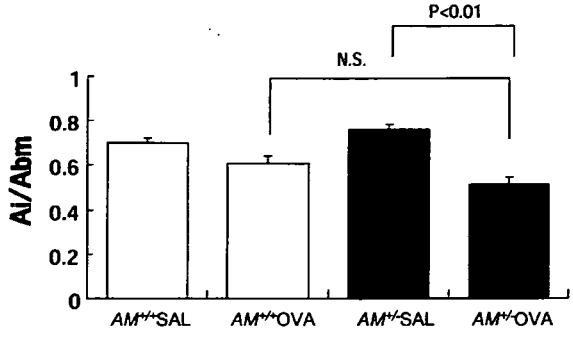

Fig. 7. Area of internal airway lumen (Ai/Abm) following OVA or SAL inhalational challenge. Ai/Abm indicates the standardized internal airway lumen area by Abm. *P* values are shown where significant ($P < 0.05$).

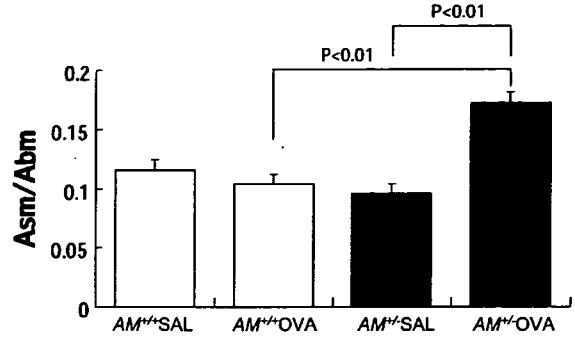

Fig. 9. Area of airway smooth muscle cell layer (Asm/Abm) following OVA or SAL inhalational challenge. Asm/Abm indicates the standardized area of airway smooth muscle cell layer by Abm. *P* values are shown where significant ($P < 0.05$).

may indicate that the tissue ADM expression could be enhanced by MCh challenge to protect against the airway contraction while ADM secretion of the mutant is so restricted that the mice could not react fully against MCh inhalation challenge. As a result, ADM-induced bronchodilation after MCh challenge could not occur thoroughly in the mutant. Since we found that altered ADM gene function is associated with AHR in allergen-induced asthma model, we then examined possible mechanisms of enhanced AHR in the mice.

First, we examined the roles of eosinophilic inflammation on AHR in the mice. Current experiments showed that eosinophils infiltrated markedly along the airways of the OVA-treated mice irrespective to ADM gene modulation. In asthma, a chronic inflammatory process of the airways leads to the development of airflow limitation and AHR. Extensive cellular infiltration is seen around the asthmatic airway. Particularly, airway eosinophilia is one of the most common features in asthmatic subjects and could be involved in bronchial hyperresponsiveness (5, 16). Although vasoactive peptides including ADM might affect airway inflammation after antigen challenge, our results indicate that the disruption of ADM gene has greater effects on AHR but little effect on antigen-induced airway eosinophilia in mice.

Second, we examined the potential proinflammatory mediators including immunoglobulins (OVA-specific IgE and IgG1), Th1 and Th2 cytokines, and LTs. In the current study, OVA-specific IgE in serum was not detected in each group, and the total IgE in BALF was not significantly different between the OVA-treated wild-type mice and the OVA-treated mutant mice. Th1 subtype preferentially produces IL-2, stimulating T lymphocyte proliferation, TNF-β, and IFN-γ that inhibit B lymphocyte activation and IgE synthesis. We examined IFN-γ as a Th1 cytokine, but no evidence was found suggesting its participation. Meanwhile, the OVA-specific IgG1, which is synthesized through Th1 and Th2 pathway, was not significantly suppressed in the serum of OVA-treated mutant mice. These findings indicate that the modulation of ADM gene might not affect IgE production mechanism through Th1 pathway. We also measured IL-4 and IL-5 that could evoke Th2 immune system, and no difference was found in the levels of IL-4 or IL-5 between the wild-type and the mutant animals, suggesting that the activation of Th2 pathway cannot be evoked by ADM insufficiency. Furthermore, cysteinyl LTs (LTC_4, LTD_4, and Lte_4) levels were not different between mutant mice and wild-type mice. Although cysteinyl LTs are reported to be one of the most important targets to treat bronchial asthma, they may not contribute to the AHR that is associated with ADM gene modulation.

Third, we investigated the morphological alteration of airways in the mice. Based on the fact the biochemical parameters do not primarily contribute to increase AHR in the mice, there may be another mechanism for AHR in the ADM-deficient mice. Histologically, OVA-treated airway specimen presents mucus hypersecretion involving hyperplasia of goblet cells and submucosal gland cells, which is compatible with the airways of asthmatic subjects. Therefore, goblet cell hyperplasia and associated mucus hypersecretion might be one of the important

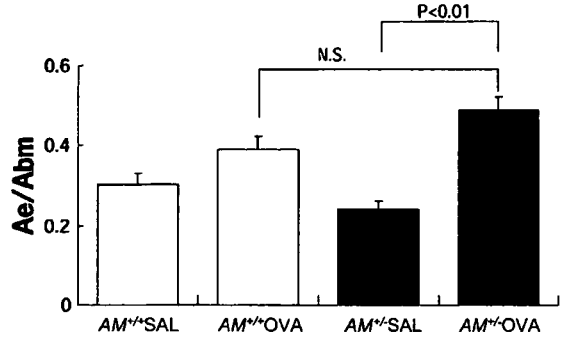

Fig. 8. Area of airway epithelial cell layer (Ae/Abm) following OVA or SAL inhalational challenge. Ae/Abm indicates the standardized area of airway epithelial cell layer by Abm. *P* values are shown where significant ($P < 0.05$).

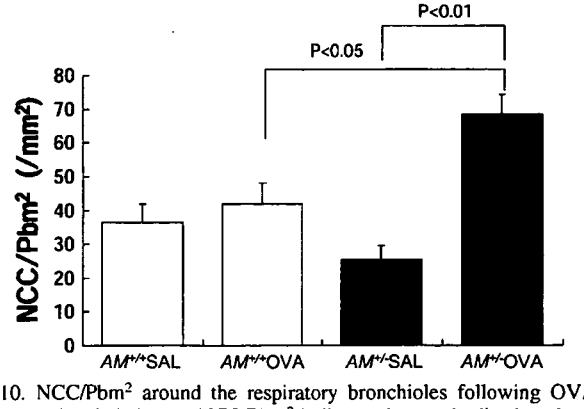

Fig. 10. NCC/Pbm^2 around the respiratory bronchioles following OVA or SAL inhalational challenge. NCC/Pbm^2 indicates the standardized nuclear cell count by Abm. *P* values are shown where significant ($P < 0.05$).

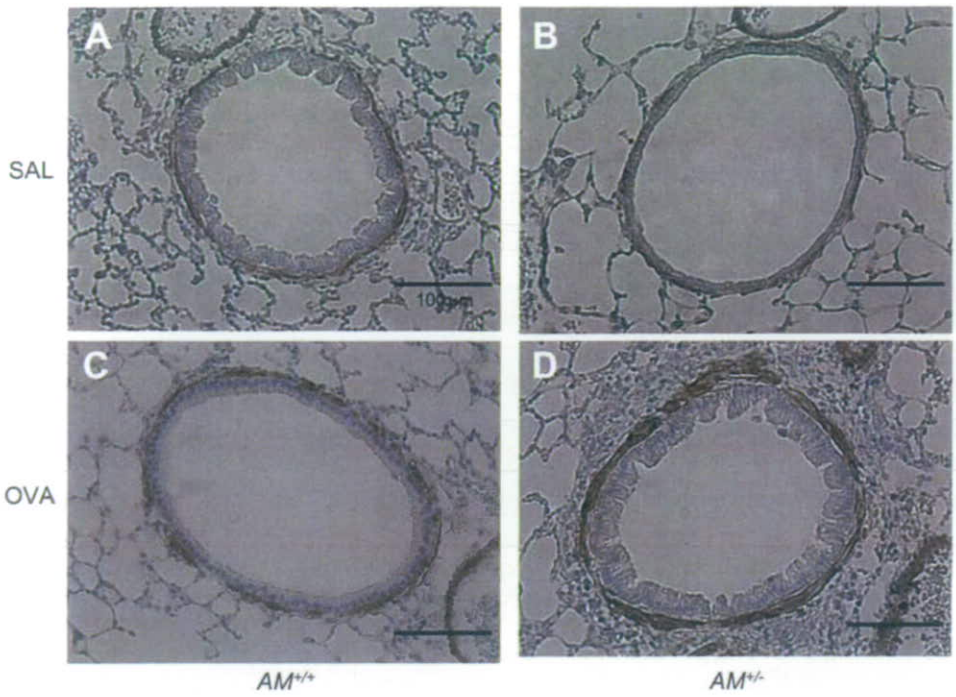

Fig. 11. Photomicrographs of small airways and lung parenchyma from saline-treated wild-type (*A*), saline-treated ADM mutant (*B*), OVA-treated wild-type (*C*), and OVA-treated ADM mutant mice (*D*) after OVA or SAL inhalational challenge. Specimens were stained with anti-α-SM actin antibody immunohistochemically. Scale bar, 100 μm.

factors of the airflow limitation and AHR in this animal model. To make this point clear, we stained each lung section by PAS and Alcian blue co-staining (PAS/Alcian blue). OVA-treated animals showed the goblet cell hyperplasia and hypersecretion as indicated by the considerable staining with PAS/Alcian blue. This phenomenon was consistently observed in the animals with OVA challenge but was not related to the ADM gene disruption, suggesting that goblet cell hyperplasia itself does not contribute the AHR in this animal model. However, our morphometric analysis data on each histological section revealed that the internal airway lumen area (Ai/Abm) of the OVA-treated mutant mice was significantly smaller than that of the OVA-untreated mutant mice. However, it was not different from that of the wild-type mice. Therefore, the thickening of airway epithelial cell layer cannot clearly explain greater airway responsiveness of the mutant mice.

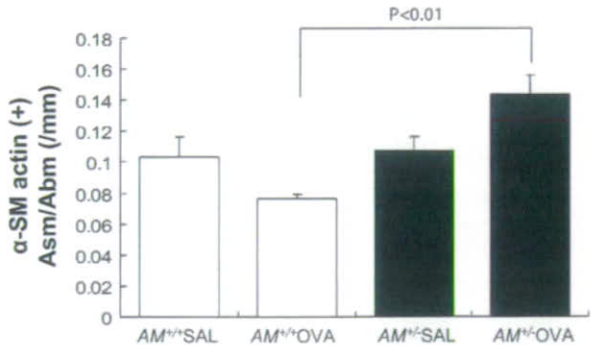

Fig. 12. Area of airway smooth muscle cell layer (Asm/Abm) following OVA or SAL inhalational challenge in the immunohistochemically stained sections with anti-α-SM actin antibody. *P* values are shown where significant ($P < 0.05$).

ADM gene is known to induce the vaso-muscle relaxation and inhibit muscle cell proliferation. The ADM gene insufficiency may be involved in the airway wall integrity in terms of cell kinetics and muscle tones. In fact, the area of the airway smooth muscle cell layer (Asm/Abm) was larger in the sensitized mutant mice than that in the sensitized wild-type mice. The peribronchial trophic changes of airway smooth muscle cells may be a primary mechanism of the current allergen-induced asthma model mice. We confirmed the ADM deficiency increases airway smooth muscle cell proliferation by using immunohistochemical staining of α-SM actin in the mouse airways. These results are consistent with the increase of nuclear cells around the basement membrane in the mice.

In this study, we did not perform an in vitro experiment concerning the effects of extracellular ADM on the airway smooth muscle proliferation. However, there are plenty of data about the inhibitory effects of ADM on smooth muscle cell proliferation in vitro and in vivo. Rossi and coworkers have demonstrated that ADM exhibits a potent dose-dependent inhibiting effect on angiotensin II (AngII)-induced human aorta smooth muscle cell proliferation and a stimulatory effect on proliferation of quiescent cells (22). Rauma-Pinola and coworkers have demonstrated that AM overexpression inhibits neointimal smooth muscle cells' growth and enhances apoptosis of the neointimal smooth muscle cells (21). It has been also reported that AM contributes to reduction of neointima formation by the inhibition of vascular smooth muscle cell proliferation via cGMP-dependent signaling pathway (1). Furthermore, ADM has an inhibitory effect on aldosterone-induced cell proliferation of adventitia in rats. This indicates that ADM may inhibit cell proliferation of both smooth muscle cells and fibroblasts in vivo (9). Consistently, it has been reported that

ADM inhibits aldosterone-induced fibroblast proliferation and ERK activity in vitro (10). Thus it may be reasonable to speculate that ADM inhibits bronchoconstrictive stress-induced cell proliferation of both smooth muscle cells and fibroblasts.

In addition, it has been reported that ADM causes the relaxation of vascular smooth muscle cells, which is associated with the intracellular cyclic AMP formation via G protein-coupled adenylate cyclase pathway (8, 14). Although the similar effects of ADM on the airway smooth muscles have not been proved yet, ADM deficiency may be associated with the less muscle relaxation through lower levels of intracellular cyclic AMP formation.

In conclusion, heterozygous ADM-deficient mice showed greater MCh-induced airway responsiveness. This is the first study that allergen-induced AHR is augmented by ADM gene disruption. Impairment of ADM gene expression does not affect airway inflammation, including eosinophilic infiltration. The airway mucus secretion, IgE synthesis, Th1 or Th2 cytokines, and cysteinyl LTs were not affected by the ADM gene modulation either. On the other hand, ADM insufficiency caused considerable airway smooth muscle hyperplasia probably due to promotion of peribronchial smooth muscle cell proliferation in the lungs. Thus ADM gene may be related to the antigen-induced airway responsiveness in association with airway smooth muscle proliferation. Furthermore, ADM might be a candidate for the novel therapeutic agent to prevent airway remodeling and asthmatic death in severe asthma. The ADM mutant mice used in this study may contribute to the study regarding the genetic roles of ADM on airway wall thickening in severe bronchial asthma and may further provide novel insights to study the physiological role of ADM in vivo.

ACKNOWLEDGMENTS

We are grateful to S. Ishii (Department of Biochemistry and Molecular Biology, Graduate School of Medicine, University of Tokyo) and T. Yokomizo (Department of Medical Biochemistry, Graduate School of Medicine, University of Kyusyu) for excellent technical assistance and valuable suggestions. We are also grateful to R. Nagai (Department of Cardiovascular Medicine, Graduate School of Medicine, University of Tokyo) for great assistance.

GRANTS

This work was supported in part by grants-in-aid for Scientific Research from the Ministry of Education, Science, Sports and Culture of Japan (no. 16590737), for the Respiratory Failure Research Group from the Ministry of Health, Labour and Welfare, Japan, and for Comprehensive Research on Aging and Health from the Ministry of Health, Labour and Welfare, Japan.

REFERENCES

1. **Agata J, Zhang JJ, Chao J, Chao L.** Adrenomedullin gene delivery inhibits neointima formation in rat artery after balloon angioplasty. *Regul Pept* 112: 115–120, 2003.
2. **Aoki-Nagase T, Nagase T, Oh-Hashi Y, Shindo T, Kurihara Y, Yamaguchi Y, Yamamoto H, Tomita T, Ohga E, Nagai R, Kurihara H, Ouchi Y.** Attenuation of antigen-induced airway hyperresponsiveness in CGRP-deficient mice. *Am J Physiol Lung Cell Mol Physiol* 283: L963–L970, 2002.
3. **Ceyhan BB, Karakurt S, Hekim N.** Plasma adrenomedullin levels in asthmatic patients. *J Asthma* 38: 221–227, 2001.
4. **Hansel NN, Diette GB.** Gene expression profiling in human asthma. *Proc Am Thorac Soc* 4: 32–36, 2007.
5. **Hogg JC.** Pathology of asthma. *J Allergy Clin Immunol* 92: 1–5, 1993.
6. **Holgate ST.** The epidemic of allergy and asthma. *Nature* 402: 2–4, 1999.
7. **Ichiki Y, Kitamura K, Kangawa K, Kawamoto M, Matsuo H, Eto T.** Distribution and characterization of immunoreactive adrenomedullin in human tissue and plasma. *FEBS Lett* 338: 6–10, 1994.
8. **Ishizaka Y, Ishizaka Y, Tanaka M, Kitamura K, Kangawa K, Minamino N, Matsuo H, Eto T.** Adrenomedullin stimulates cyclic AMP formation in rat vascular smooth muscle cells. *Biochem Biophys Res Commun* 200: 642–646, 1994.
9. **Jiang W, Yang JH, Pan CS, Qi YF, Pang YZ, Tang CS.** Effects of adrenomedullin on cell proliferation in rat adventitia induced by aldosterone. *J Hypertens* 22: 1953–1961, 2004.
10. **Jiang W, Yang JH, Wang SH, Pan CS, Qi YF, Zhao J, Tang CS.** Effects of adrenomedullin on aldosterone-induced cell proliferation in rat cardiac fibroblasts. *Biochim Biophys Acta* 1690: 265–275, 2004.
11. **Kanazawa H, Kawaguchi T, Fujii T, Kudoh S, Hirata K, Kurihara N, Takeda T.** Comparison of bronchodilator responses to adrenomedullin and proadrenomedullin N-terminal 20 peptide. *Life Sci* 57: 241–245, 1995.
12. **Kanazawa H, Kurihara N, Hirata K, Kudoh S, Kawaguchi T, Takeda T.** Adrenomedullin, a newly discovered hypotensive peptide, is a potent bronchodilator. *Biochem Biophys Res Commun* 205: 251–254, 1994.
13. **Kitamura K, Ichiki Y, Tanaka M, Kawamoto M, Emura J, Sakakibara S, Kangawa K, Matsuo H, Eto T.** Immunoreactive adrenomedullin in human plasma. *FEBS Lett* 341: 288–290, 1994.
14. **Kitamura K, Kangawa K, Kawamoto M, Ichiki Y, Nakamura S, Matsuo H, Eto T.** Adrenomedullin: a novel hypotensive peptide isolated from human pheochromocytoma. *Biochem Biophys Res Commun* 192: 553–560, 1993.
15. **Kung TT, Jones H, Adams GK 3rd, Umland SP, Kreutner W, Egan RW, Chapman RW, Watnick AS.** Characterization of a murine model of allergic pulmonary inflammation. *Int Arch Allergy Immunol* 105: 83–90, 1994.
16. **McFadden ER Jr, Gilbert IA.** Asthma. *N Engl J Med* 327: 1928–1937, 1992.
17. **McLatchie LM, Fraser NJ, Main MJ, Wise A, Brown J, Thompson N, Solari R, Lee MG, Foord SM.** RAMPs regulate the transport and ligand specificity of the calcitonin-receptor-like receptor. *Nature* 393: 333–339, 1998.
18. **Nagase T, Ishii S, Shindou H, Ouchi Y, Shimizu T.** Airway hyperresponsiveness in transgenic mice overexpressing platelet activating factor receptor is mediated by an atropine-sensitive pathway. *Am J Respir Crit Care Med* 165: 200–205, 2002.
19. **Nagase T, Matsui H, Aoki T, Ouchi Y, Fukuchi Y.** Lung tissue behavior in the mouse during constriction induced by methacholine and endothelin-1. *J Appl Physiol* 81: 2373–2378, 1996.
20. **Ohbayashi H, Suito H, Yoshida N, Ilto Y, Kume H, Yamaki K.** Adrenomedullin inhibits ovalbumin-induced bronchoconstriction and airway microvascular leakage in guinea-pigs. *Eur Respir J* 14: 1076–1081, 1999.
21. **Rauma-Pinola T, Paakko P, Ilves M, Serpi R, Romppanen H, Vuolteenaho O, Ruskoaho H, Hautala T.** Adrenomedullin gene transfer induces neointimal apoptosis and inhibits neointimal hyperplasia in injured rat artery. *J Gene Med* 8: 452–458, 2006.
22. **Rossi F, Bertone C, Petricca S, Santiemma V.** Adrenomedullin antagonizes angiotensin II-stimulated proliferation of human aortic smooth muscle cells. *Peptides* 27: 2935–2941, 2006.
23. **Shindo T, Kurihara Y, Nishimatsu H, Moriyama N, Kakoki M, Wang Y, Imai Y, Ebihara A, Kuwaki T, Ju KH, Minamino N, Kangawa K, Ishikawa T, Fukuda M, Akimoto Y, Kawakami H, Imai T, Morita H, Yazaki Y, Nagai R, Hirata Y, Kurihara H.** Vascular abnormalities and elevated blood pressure in mice lacking adrenomedullin gene. *Circulation* 104: 1964–1971, 2001.

Respirology (2007) **12**, 807–813 doi: 10.1111/j.1440-1843.2007.01172.x

ORIGINAL ARTICLE

Calcitonin gene-related peptide mediates acid-induced lung injury in mice

TOMOKO AOKI-NAGASE,[1] TAKAHIDE NAGASE,[2*] YOSHIO OH-HASHI,[3] YUKIKO KURIHARA,[3] YASUHIRO YAMAGUCHI,[1] HIROSHI YAMAMOTO,[1] TAIJI NAGATA,[2] HIROKI KURIHARA[3] AND YASUYOSHI OUCHI[1]

Departments of [1]Geriatric Medicine, [2]Respiratory Medicine, and [3]Physiological Chemistry and Metabolism, Graduate School of Medicine, University of Tokyo, Tokyo, Japan

Calcitonin gene-related peptide mediates acid-induced lung injury in mice
AOKI-NAGASE T, NAGASE T, OH-HASHI Y, KURIHARA Y, YAMAGUCHI Y, YAMAMOTO H, NAGATA T, KURIHARA H, OUCHI Y. *Respirology* 2007; **12**: 807–813

Background and objective: Acid-induced lung injury from aspiration is one of the most important causes of ARDS. Calcitonin gene-related peptide (CGRP) is a neuropeptide that has various biological actions. The current study investigated whether CGRP might have pathophysiological roles in acid-induced lung injury.

Methods: The investigations employed CGRP gene-disrupted mice—mutant mice ($CGRP^{-/-}$) and their littermate controls ($CGRP^{+/+}$). Anaesthetized and mechanically ventilated mice received 2 mL/kg HCl (pH = 1.5) intratracheally. Lung wet-to-dry weight ratios were calculated to assess pulmonary oedema, total and differential cell counts of the BALF were determined, and measurements of myeloperoxidase activity were performed.

Results: Acid-induced lung injury was characterized by an increase in lung permeability and respiratory failure. Disruption of the CGRP gene significantly attenuated acid-induced injury, oedema and respiratory failure.

Conclusions: This study suggests that CGRP is involved in the pathogenesis of acute lung injury caused by acid aspiration and CGRP mutant mice may provide an appropriate model to study molecular mechanisms in this context.

Key words: acid aspiration, acute lung injury, acute respiratory distress syndrome, calcitonin gene-related peptide, knockout mice.

INTRODUCTION

ARDS is an acute lung injury, with a mortality ranging from 40% to 70% despite intensive care. Acid-induced injury from aspiration is one of the most important causes of ARDS. A potential mechanism for the acid-associated lung injury includes: (i) hydrochloric acid (HCl)-induced damage to the alveolar-capillary membrane; and (ii) polymorphonuclear neutrophil (PMN) adhesion, activation and sequestration, leading to pulmonary oedema and deterioration of gas exchange.[1,2]

Calcitonin gene-related peptide (CGRP), a 37-amino-acid peptide, is a neuropeptide that has various biological actions, including responses to sensory stimuli, cardiovascular regulation and vasodilation.[3–6] There are two CGRP isoforms, αCGRP and βCGRP. αCGRP is present in the central and peripheral nervous systems,[7] while βCGRP is expressed in specific neuronal sites.[8] In the respiratory system, CGRP is synthesized by sensory C-fibres throughout the respiratory tree[9,10] and is reported to be involved in the regulation of airway physiology.[11,12] CGRP is also found in neuroepithelial cells of the lung and coexists with tachykinins in many airway sensory nerves,[13] while CGRP receptors are found in lung vessels.[14] It has been shown that CGRP, a potent

Correspondence: Tomoko Aoki-Nagase, Department of Respiratory Medicine, Graduate School of Medicine, University of Tokyo, 7-3-1 Hongo, Bunkyo-ku, Tokyo 113-8655, Japan. Email: takahide-tky@umin.ac.jp

*Takahide Nagase, being an Associate Editor for *Respirology*, did not influence the outcome of this manuscript.

Received 11 December 2006; invited to revise 23 January 2007; revised 28 January 2007; accepted 5 March 2007 (Associate Editor: Yoichi Nakanishi).

vasodilator,[15] modulates hypoxic pulmonary vasoconstriction.[10] Recent studies using genetically engineered mice have shown that CGRP knockout mice exhibit increased blood pressure and overactivation of their sympathetic nervous system.[16] In terms of its physiological role in the lung, it has been reported that CGRP potently constricts airway smooth muscle in humans[17] and guinea pigs.[18] In addition, it has been shown that CGRP may have a significant role in eosinophilia in allergic inflammation.[19,20] Based on these observations, it is assumed that CGRP might be involved in other inflammatory responses in the lung.

The current study investigated whether αCGRP might have pathophysiological roles in a murine model of acid-induced lung injury due to acid aspiration. CGRP gene-disrupted mice were used in the study.[16]

METHODS

Mice

αCGRP-null mice were established as previously reported.[16] Briefly, the mouse *CT/αCGRP* genomic DNA was cloned from a BALB/c mouse genomic library in EMBL3 using synthetic oligonucleotide probes derived from the mouse *CT/αCGRP* cDNA sequence. A 7.0-kb fragment containing exons 3–5 of the mouse *CT/αCGRP* gene was subcloned into pBluescript (Stratagene, Santa Clara, CA, USA). A targeting vector was constructed by replacing the 1.6-kb *XbaI–XbaI* fragment encompassing exon 5, which is specific for *αCGRP*, with the neomycin-resistance gene, and by flanking the thymidine kinase gene. This plasmid was linearized with *NotI* and introduced into 129/Sv-derived SM-1 ES cells by electroporation, after which the cells were selected in medium containing G418 and ganciclovir. Homologous recombinants were identified by PCR and Southern blot analysis. Targeted ES cell clones were injected into C57BL/6 mouse blastocysts to generate chimeric mice. Male chimeras were then crossbred with C57BL/6 females, and germline transmission was achieved. Mice heterozygous for αCGRP mutant allele with the genetic background of the 129/Sv × C57BL/6 hybrid were mated. Offspring were genotyped at 4 weeks of age. For genotyping, genomic DNAs were isolated from biopsied tail and subjected to PCR amplification. Mice were fed with a standard laboratory diet and water *ad libitum*. CGRP knockout mice ($\alpha CGRP^{-/-}$) and their littermate wild-type mice ($\alpha CGRP^{+/+}$) were used in the current study.

Protocols

Animals were anaesthetized with pentobarbital sodium (25 mg/kg, ip) and ketamine hydrochloride (25 mg/kg, ip) in combination and then paralysed with pancuronium bromide (0.3 mg/kg, ip). Anaesthesia and paralysis were maintained by supplemental administration of 10% of the initial dose every hour. After tracheostomy, an endotracheal metal tube (inside diameter of 1 mm, length of 8 mm) was inserted in the trachea. Animals were mechanically ventilated (model 683, Harvard Apparatus, South Natick, MA, USA) with tidal volumes of 10 mL/kg and frequencies of 2.5 Hz. The thorax was widely opened by means of midline sternotomy, and a PEEP of 2 cm H_2O was applied by placing the expiratory line underwater.

One minute prior to aspiration challenge, two deep inhalations (3 times tidal volume) were delivered to standardize volume, and measurements were made to obtain baseline values. Then, the anaesthetized and mechanically ventilated mice received 2 mL/kg HCl (pH = 1.5) intratracheally, followed by a bolus of air (30 mL/kg). In the control group, animals received saline instead of HCl in the same manner. We therefore studied four groups: saline-treated wild-type, saline-treated knockout, HCl-treated wild-type, and HCl-treated knockout groups ($n = 5$, respectively, for each group). In all groups, measurements were made at 30-min intervals for 2 h. To assess the development of physiological lung injury, elastance (EL, a reciprocal of lung compliance) was measured as previously described.[21–27] Briefly, we measured the tracheal pressure (Ptr), flow and volume (V). EL and lung resistance (RL) were calculated by adjusting the equation of motion: $Ptr = EL\,V + RL\,(dV/dt) + K$, where K was a constant. Changes in EL reflect lung parenchymal alterations and stiffening of the lungs.[28,29] At the end of the experiment, animals were sacrificed by exsanguination.

Assessment of respiratory failure

At the end of the experiment, blood samples from the left ventricle were used to obtain measurements of PaO_2, $PaCO_2$ and pH.

Assessment of pulmonary oedema

At the end of the experiment, the lung wet-to-dry weight ratios were calculated to assess pulmonary oedema. After the trapped blood was drained from the excised lungs, the lung wet weight was measured. The lungs were then heated at 90°C to constant weight in a gravity convection oven for 72 h, and the residuum was taken as the lung dry weight.

BALF

At the end of the experiment, BAL was performed (1 mL of PBS × 5) in each group. The BALF was centrifuged at 450 *g* for 10 min, and the total and differential cell counts of the BALF were determined from the cell fraction. The supernatant was stored at −70°C until the protein was determined. The concentration of protein was measured by Lowry's method using BSA as standard.

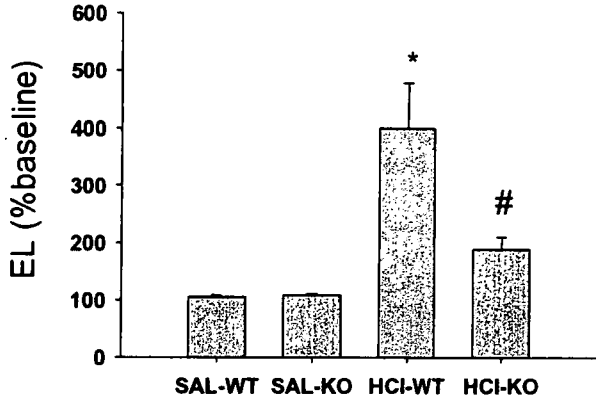

Figure 1 Roles of the CGRP gene in acid-induced lung injury. Changes in lung elastance (EL) in CGRP knockout mice ($\alpha CGRP^{-/-}$) and wild-type mice ($\alpha CGRP^{+/+}$) 2 h after aspiration of either HCl or saline ($n = 5$). *$P < 0.01$ versus saline-treated groups. #$P < 0.01$ versus HCl-treated wild-type group and saline-treated groups. HCl-KO, HCl-treated knockout mice; HCl-WT, HCl-treated wild-type mice; SAL-KO, saline-treated knockout mice; SAL-WT, saline-treated wild-type mice.

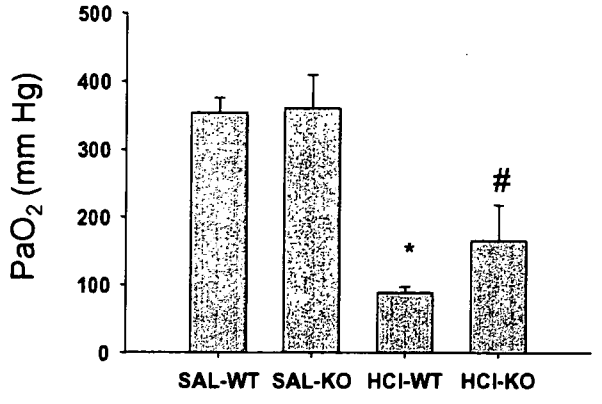

Figure 2 Roles of the CGRP gene in acid-induced hypoxaemia. PaO_2 level 2 h after aspiration ($n = 4$). Responses following the administration of HCl or saline are shown. *$P < 0.01$ versus saline-treated groups. #$P < 0.05$ versus HCl-treated wild-type group and saline-treated groups. HCl-KO, HCl-treated knockout mice; HCl-WT, HCl-treated wild-type mice; SAL-KO, saline-treated knockout mice; SAL-WT, saline-treated wild-type mice.

Myeloperoxidase (MPO) activity assay

At the end of experiments, the left lungs of the mice were removed in each group. Measurements of MPO activity were performed as reported.[30,31]

Data analysis

Comparisons of experimental groups were carried out using the Kruskal–Wallis test. Data are expressed as mean ± SD. *P*-values of <0.05 were considered significant.

RESULTS

HCl-induced changes in EL and RL in $\alpha CGRP^{-/-}$ mice were significantly less than the wild-type controls ($n = 5$ for each group; Fig. 1 and Table 1). Figure 1 demonstrates the responses in lung elasticity in the HCl- and saline-treated groups.

HCl-treated groups showed deterioration of gas exchange; however, HCl-induced hypoxaemia was significantly attenuated in CGRP mutant mice ($n = 4$ for each group; Fig. 2). HCl treatment induced significant increases in $PaCO_2$ and decreases in pH in the wild-type mice compared with the knockout mice (Table 1).

To assess the severity of lung oedema, lung wet-to-dry weight ratios were measured in each group ($n = 3$–4 for each group; Fig. 3). Lung wet-to-dry weight ratio in HCl-treated $\alpha CGRP^{-/-}$ mice was significantly decreased compared with wild-type HCl-treated mice.

HCl administration increased the amount of protein in BALF, indicating HCl-induced protein leakage ($n = 4$ for each group; Fig. 4). As shown, HCl-induced protein leakage was significantly attenuated in CGRP mutant mice. Total cell counts and differential cell fractions are summarized in Table 2. HCl administration increased the total cell counts and the number of PMN in BALF. However, HCl aspiration elicited no significant differences in PMN infiltration between the wild-type and $\alpha CGRP^{-/-}$ mice ($n = 4$ for each group; Fig. 5).

To assess the PMN infiltration in the lung, MPO activity assay was performed. Figure 6 shows the results of MPO activity in lung tissue. No significant difference in lung MPO activity was observed between the wild-type and $\alpha CGRP^{-/-}$ mice ($n = 3$–4 for each group).

Table 1 Lung resistance (RL), $PaCO_2$ and pH levels (mean ± SD) 2 h after aspiration in the experimental and control groups of mice

	RL (%baseline)	$PaCO_2$ (mm Hg)	pH
SAL-WT	100.3 ± 1.8	32.8 ± 7.6	7.46 ± 0.10
SAL-KO	100.3 ± 3.6	29.3 ± 7.7	7.50 ± 0.05
HCl-WT	128.5 ± 5.2*	45.8 ± 11.0*	7.17 ± 0.12*
HCl-KO	108.6 ± 5.9**	36.8 ± 2.2**	7.34 ± 0.09**

*$P < 0.05$ versus saline-treated groups; **$P < 0.05$ versus HCl-treated wild-type group, not significant versus saline-treated groups.

HCl-KO, HCl-treated knockout mice; HCl-WT, HCl-treated wild-type mice; SAL-KO, saline-treated knockout mice; SAL-WT, saline-treated wild-type mice.

DISCUSSION

The results of the current study suggest that CGRP is involved in the development of acid-induced lung

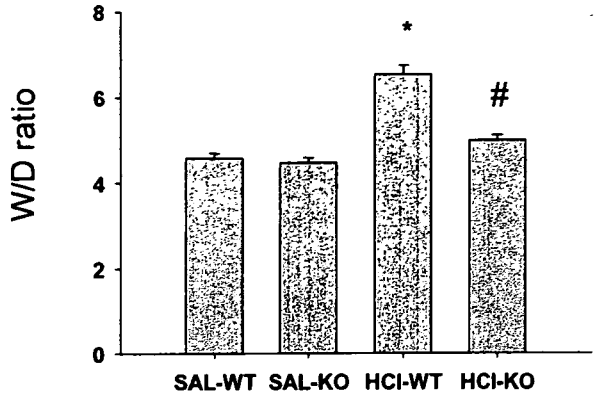

Figure 3 Roles of the CGRP gene in acid-induced lung oedema. The lung wet-to-dry weight (W/D) ratio 2 h after aspiration ($n = 3$–4). Responses following the administration of HCl or saline are shown. *$P < 0.05$ versus saline-treated groups. #$P < 0.05$ versus HCl-treated wild-type group. HCl-KO, HCl-treated knockout mice; HCl-WT, HCl-treated wild-type mice; SAL-KO, saline-treated knockout mice; SAL-WT, saline-treated wild-type mice.

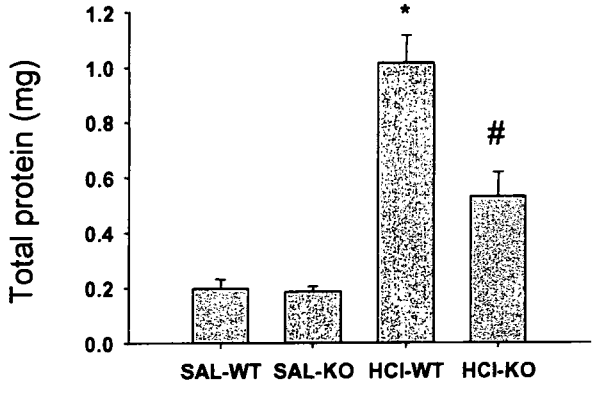

Figure 4 Roles of the CGRP gene in acid-induced protein leakage. Total protein amounts of BALF 2 h after aspiration ($n = 4$). Responses following the administration of HCl or saline are shown. *$P < 0.01$ versus saline-treated groups. #$P < 0.01$ versus HCl-treated wild-type group and saline-treated groups. HCl-KO, HCl-treated knockout mice; HCl-WT, HCl-treated wild-type mice; SAL-KO, saline-treated knockout mice; SAL-WT, saline-treated wild-type mice.

injury. Disruption of the CGRP gene significantly attenuated lung water and presumably tissue oedema—and respiratory failure. However, PMN sequestration was not regulated by CGRP. These observations indicate that CGRP may mediate certain key features of acid-induced lung injury.

CGRP belongs to the calcitonin family of peptides, including calcitonin, amylin and adrenomedullin. The calcitonin-receptor-like receptor functions as a CGRP receptor in the presence of receptor-activity-modifying protein 1.[32] CGRP has pleiotropic and pathophysiological effects on various cells and organs,[10] and exerts trophic effects on skeletal muscle and vascular smooth muscle.[4] CGRP also modulates some macrophage functions, including antigen presentation.[33,34] In the respiratory system, CGRP is synthesized by sensory C-fibres in the respiratory tree.[9] Based on the biological effects of CGRP, it has been suggested that CGRP might be related to the pathogenesis of inflammatory diseases, including bronchial asthma and acute lung injury. Recent studies using genetically engineered mice have shown that CGRP knockout mice exhibit attenuation of antigen-induced airway hyperresponsiveness.[35] It has been demonstrated that CGRP potently constricts human airway smooth muscle.[17] Regarding eosinophil chemotaxis, Numao and Agrawal[20] have reported that neuropeptides, including CGRP, may play a significant role in eosinophil infiltration by priming cells in allergic inflammation. In the present study, it was hypothesized that CGRP could play a significant role in the mechanism underlying acid-induced lung injury. To test this hypothesis, acid-induced pulmonary responses using αCGRP gene-disrupted mice, which have been recently established by Oh-hashi *et al.*,[16] were studied.

Aspiration of gastric contents is reported to be associated with an ARDS incidence of 26–36%.[36] Acute lung injury induced by massive acid aspiration is characterized by increased permeability in the lung, decreased lung compliance, enhanced PMN sequestration and respiratory failure. In this study, acid-induced lung oedema and respiratory failure were significantly attenuated in the αCGRP-deficient mice, suggesting that the presence of CGRP *per se* is associated with acid-induced lung injury. This is the first report that CGRP could be involved in the acute lung injury using a murine model. Based on the report that CGRP knockout mice exhibit increased blood pressure and overactivation of the sympathetic nervous system,[16] disruption of the CGRP gene could affect pulmonary vascular permeability with consequent attenuated lung oedema induced by acid challenge. However, the exact mechanism to explain the involvement of CGRP in acid-induced lung injury is unclear.

One possible mechanism is that CGRP might affect pulmonary inflammation, including PMN infiltration, after acid challenge. Neutrophil sequestration is a common feature of ARDS subjects. In the current study, however, no significant difference in BALF PMN count or lung MPO activity was observed between the wild-type and CGRP-deficient mice. These results suggest that the disruption of the CGRP gene has little effect on acid-induced neutrophilia in mice.

Acid-induced alterations in lung elastance, PaO_2 and BALF protein were not completely eliminated in CGRP mutant mice, although they were markedly attenuated compared with the HCl-treated wild-type group. These observations suggest that factors other than CGRP also play a role and contribute to physiological alteration in the development of acute lung injury. It has been postulated that platelet-activation factor (PAF), eicosanoids, adhesion molecules and cytokines are also involved in this mechanism.[21,37] Considering that there are as yet no drugs to manage

Table 2 Total cell counts and cell fractions (mean ± SD) in BALF 2 h after aspiration in the experimental and control groups

	Total cell counts ($\times 10^5$)	Macrophage (%)	PMN (%)	Lymphocyte (%)
SAL-WT	1.11 ± 0.89	95.5 ± 0.3	0.5 ± 0.4	4.0 ± 0.7
SAL-KO	1.03 ± 0.68	95.0 ± 0.4	0.3 ± 0.5	4.8 ± 0.5
HCl-WT	3.55 ± 0.34*	94.0 ± 0.6	2.4 ± 1.0*	3.6 ± 1.4
HCl-KO	3.37 ± 0.30**	95.1 ± 0.3	2.1 ± 0.6**	2.8 ± 0.6

*$P < 0.01$ versus saline-treated groups; **$P < 0.01$ versus saline-treated groups, not significant versus HCl-treated wild-type group.

HCl-KO, HCl-treated knockout mice; HCl-WT, HCl-treated wild-type mice; PMN, polymorphonuclear neutrophil; SAL-KO, saline-treated knockout mice; SAL-WT, saline-treated wild-type mice.

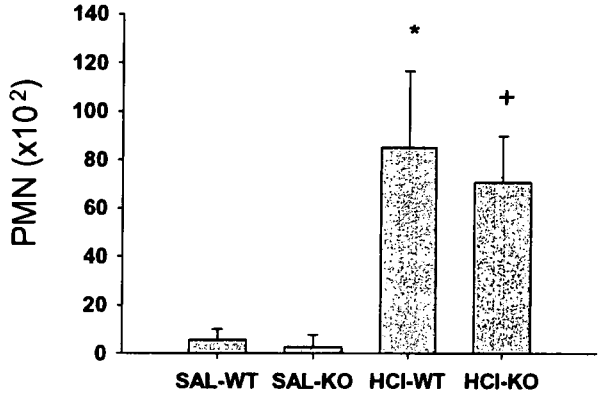

Figure 5 Roles of the CGRP gene in acid-induced neutrophil infiltration. Polymorphonuclear neutrophil (PMN) counts of BALF 2 h after aspiration ($n = 4$). Responses following the administration of HCl or saline are shown. *$P < 0.01$ versus saline-treated groups. +$P < 0.01$ versus saline-treated groups, not significant versus HCl-treated wild-type group. HCl-KO, HCl-treated knockout mice; HCl-WT, HCl-treated wild-type mice; SAL-KO, saline-treated knockout mice; SAL-WT, saline-treated wild-type mice.

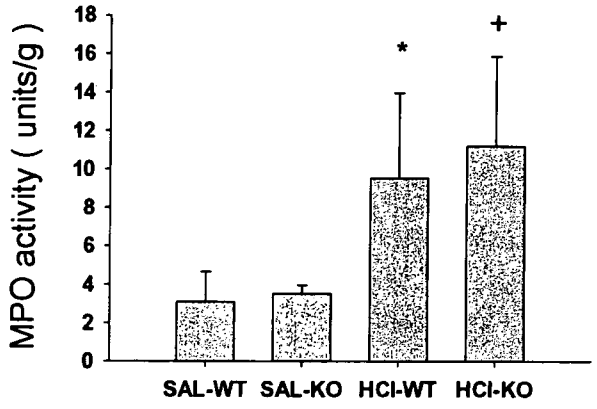

Figure 6 Roles of the CGRP gene in acid-induced neutrophil infiltration. Myeloperoxidase (MPO) activity assay in the lung 2 h after aspiration ($n = 3$–4). Responses following the administration of HCl or saline are shown. *$P < 0.01$ versus saline-treated groups. +$P < 0.01$ versus saline-treated groups, not significant versus HCl-treated wild-type group. HCl-KO, HCl-treated knockout mice; HCl-WT, HCl-treated wild-type mice; SAL-KO, saline-treated knockout mice; SAL-WT, saline-treated wild-type mice.

pulmonary oedema and improve survival rates, these mediators are possible targets for the development of therapeutic agents. The CGRP mutant mice used in this study may be useful to study the role of CGRP in inflammatory disorders and may provide novel insights into the pathophysiological roles of CGRP and the CGRP gene *in vivo*.

An important shortcoming of our studies is that we did not perform detailed studies of mouse lung tissue responses to acid. This would have made it possible to verify vascular changes and tissue oedema, and would have provided information on the numbers of inflammatory cells present.

In summary, the disruption of the CGRP gene significantly attenuated acid-induced lung damage and respiratory failure, but did not affect PMN infiltration in a mouse model of ARDS. The current observations suggest that CGRP might be involved in the pathogenesis of acute lung injury caused by acid aspiration. CGRP mutant mice may provide appropriate models to study molecular and pathophysiological mechanisms underlying diseases related to CGRP.

ACKNOWLEDGEMENT

This work was supported in part by grants-in-aid for Scientific Research from the Ministry of Education, Science, Sports, Culture and Technology of Japan; a grant to the Respiratory Failure Research Group from the Ministry of Health, Labour and Welfare, Japan; and grants-in-aid for Comprehensive Research on Aging and Health from the Ministry of Health, Labour and Welfare, Japan. T. Aoki-Nagase is a Research Resident of Japan Foundation for Aging and Health.

REFERENCES

1 Eijking EP, Gommers D, So KL, Vergeer M, Lachmann B. Surfactant treatment of respiratory failure induced by hydrochloric acid aspiration in rats. *Anesthesiology* 1993; **78**: 1145–51.

2 Pittet JF, Mackersie RC, Martin TR, Matthay MA. Biological markers of acute lung injury: prognostic and

pathogenetic significance. *Am. J. Respir. Crit. Care Med.* 1997; **155**: 1187–205.
3 Amara SG, Jonas V, Rosenfeld MG, Ong ES, Evans RM. Alternative RNA processing in calcitonin gene expression generates mRNAs encoding different polypeptide products. *Nature* 1982; **298**: 240–4.
4 Brain SD, Williams TJ, Tippins JR, Morris HR, MacIntyre I. Calcitonin gene-related peptide is a potent vasodilator. *Nature* 1985; **313**: 54–6.
5 Lundberg JM, Anders FC, Hua X, Hökfelt T, Fischer JA. Coexistence of substance P and calcitonin gene-related peptide-like immunoreactivities in sensory nerves in relation to cardiovascular and bronchoconstrictor effects of capsaicin. *Eur. J. Pharmacol.* 1985; **108**: 315–19.
6 Lu B, Fu WM, Greengard P, Poo MM. Calcitonin gene-related peptide potentiates synaptic responses at developing neuromuscular junction. *Nature* 1993; **363**: 76–9.
7 Rosenfeld MG, Mermod JJ, Amara SG, Swanson LW, Sawchenko PE *et al.* Production of a novel neuropeptide encoded by the calcitonin gene via tissue-specific RNA processing. *Nature* 1983; **304**: 129–35.
8 Amara SG, Arriza JL, Leff SE, Swanson LW, Evans RM *et al.* Expression in brain of a messenger RNA encoding a novel neuropeptide homologous to calcitonin gene-related peptide. *Science* 1985; **229**: 1094–7.
9 Terada M, Iwanaga T, Iwanaga HT, Adachi I. Calcitonin gene-related peptide (CGRP)-immunoreactive nerves in the tracheal epithelium of rats: an immunohistochemical study by means of whole mount preparations. *Arch. Histol. Cytol.* 1992; **55**: 219–33.
10 Solway J, Leff AR. Sensory neuropeptides and airway function. *J. Appl. Physiol.* 1991; **71**: 2077–87.
11 Cadieux A, Monast NP, Pomerleau F, Fournier A, Lanoue C. Bronchoprotector properties of calcitonin-gene related peptide in guinea pig and human airways. *Am. J. Respir. Crit. Care Med.* 1999; **159**: 235–43.
12 Nagase T, Ohga E, Katayama H, Sudo E, Aoki T *et al.* Roles of calcitonin-gene related peptide (CGRP) in hyperpnea-induced constriction in guinea pigs. *Am. J. Respir. Crit. Care Med.* 1996; **154**: 1551–6.
13 Merighi A, Polak JM, Gibson SJ, Gulbenkian S, Valentino KL *et al.* Ultrastructural studies on calcitonin gene-related peptide-, tachykinins-, and somatostatin-immunoreactive neurons in rat dorsal root ganglia: evidence for the colocalization of different peptides in single secretory granules. *Cell Tissue Res.* 1988; **254**: 101–9.
14 Janssen PL, Tucker A. Calcitonin gene-related peptide modulates pulmonary vascular reactivity in isolated rat lungs. *J. Appl. Physiol.* 1994; **77**: 142–6.
15 McCormack D, Mak J, Coupe M, Barnes PJ. Calcitonin gene-related peptide vasodilation of human pulmonary vessels. *J. Appl. Physiol.* 1989; **67**: 1265–70.
16 Oh-hashi Y, Shindo T, Kurihara Y, Imai T, Wang Y *et al.* Elevated sympathetic nervous activity in mice deficient in αCGRP. *Circ. Res.* 2001; **89**: 983–90.
17 Palmer JBD, Cuss FMC, Mulderry PK, Ghatei MA, Springall DR *et al.* Calcitonin-gene related peptide is localized to human airway nerves and potently constricts human airway smooth muscle. *Br. J. Pharmacol.* 1987; **91**: 95–101.
18 Pinto A, Sekizawa K, Yamaya M, Ohrui T, Jia YX *et al.* Effects of adrenomedullin and calcitonin gene-related peptide on airway and pulmonary vascular smooth muscle in guinea-pigs. *Br. J. Pharmacol.* 1996; **119**: 1477–83.
19 Davies D, Medeiros MS, Keen J, Turner AJ, Haynes LW. Endopeptidase-24. 11 cleaves a chemotactic factor from α-calcitonin gene-related peptide. *Biochem. Pharmacol.* 1992; **43**: 1753–6.
20 Numao T, Agrawal DK. Neuropeptides modulate human eosinophil chemotaxis. *J. Immunol.* 1992; **149**: 3309–15.
21 Nagase T, Fukuchi Y, Matsuse T, Sudo E, Matsui H *et al.* Antagonism of ICAM-1 attenuates airway and tissue responses to antigen in sensitized rats. *Am. J. Respir. Crit. Care Med.* 1995; **151**: 1244–9.
22 Nagase T, Matsui H, Aoki T, Ouchi Y, Fukuchi Y. Lung tissue behaviour in the mouse during constriction induced by methacholine and endothelin-1. *J. Appl. Physiol.* 1996; **81**: 2373–8.
23 Nagase T, Kurihara H, Kurihara Y, Aoki T, Fukuchi Y *et al.* Airway hyperresponsiveness to methacholine in mutant mice deficient in endothelin-1. *Am. J. Respir. Crit. Care Med.* 1998; **157**: 560–4.
24 Nagase T, Ishii S, Shindou H, Ouchi Y, Shimizu T. Airway hyperresponsiveness in transgenic mice overexpressing platelet-activating factor receptor is mediated by an atropine-sensitive pathway. *Am. J. Respir. Crit. Care Med.* 2002; **165**: 200–5.
25 Nagase T, Ishii S, Katayama H, Fukuchi Y, Ouchi Y *et al.* Airway responsiveness in transgenic mice overexpressing platelet-activating factor receptor: roles of thromboxanes and leukotrienes. *Am. J. Respir. Crit. Care Med.* 1997; **156**: 1621–7.
26 Ishii S, Nagase T, Tashiro F, Ikuta K, Sato S *et al.* Bronchial hyperreactivity, increased endotoxin lethality and melanocytic tumorigenesis in transgenic mice overexpressing platelet-activating factor receptor. *EMBO J.* 1997; **16**: 133–42.
27 Ishii S, Kuwaki T, Nagase T, Maki K, Tashiro F *et al.* Impaired anaphylactic responses but intact sensitivity to endotoxin in mice lacking a platelet-activating factor receptor. *J. Exp. Med.* 1998; **187**: 1779–88.
28 Nagase T, Uozumi N, Ishii S, Kume K, Izumi T *et al.* Acute lung injury by sepsis and acid aspiration: a key role for cytosolic phospholipase A2. *Nat. Immunol.* 2000; **1**: 42–6.
29 Nagase T, Uozumi N, Ishii S, Kita Y, Yamamoto H *et al.* A pivotal role of cytosolic phospholipase A2 in bleomycin-induced pulmonary fibrosis. *Nat. Med.* 2002; **8**: 480–4.
30 Nagase T, Uozumi N, Aoki-Nagase T, Terawaki K, Ishii S *et al.* A potent inhibitor of cytosolic phospholipase A2, arachidonyl trifluoromethyl ketone, attenuates LPS-induced lung injury in mice. *Am. J. Physiol. Lung Cell. Mol. Physiol.* 2003; **284**: L720–6.
31 Blackwell TS, Lancaster LH, Blackwell TR, Venkatakrishnan A, Christman JW. Chemotactic gradients predict neutrophilic alveolitis in endotoxin-treated rats. *Am. J. Respir. Crit. Care Med.* 1999; **159**: 1644–52.
32 McLatchie LM, Fraser NJ, Main MJ, Wise A, Brown J *et al.* RAMPs regulate the transport and ligand specificity of the calcitonin-receptor-like receptor. *Nature* 1998; **393**: 333–9.
33 Hosoi J, Murphy GF, Egan CL, Lerner EA, Grabbe S *et al.* Regulation of Langerhans cell function by nerves containing calcitonin-gene related peptide. *Nature* 1993; **363**: 159–63.

34 Nong YH, Titus RG, Ribeiro JMC, Remold HG. Peptides encoded by the calcitonin gene inhibit macrophage function. *J. Immunol.* 1989; **143**: 45–9.
35 Aoki-Nagase T, Nagase T, Oh-hashi Y, Shindo T, Kurihara Y *et al.* Attenuation of antigen-induced airway hyperresponsiveness in CGRP-deficient mice. *Am. J. Physiol. Lung Cell. Mol. Physiol.* 2002; **283**: L963–70.
36 Hudson LD, Milberg JA, Anardi D, Maunder RJ. Clinical risks for development of the acute respiratory distress syndrome. *Am. J. Respir. Crit. Care Med.* 1995; **151**: 293–301.
37 Folkesson HG, Matthay MA, Hebert CA, Broaddus VC. Acid aspiration-induced lung injury in rabbits is mediated by interleukin-8-dependent mechanisms. *J. Clin. Invest.* 1995; **96**: 107–16.

resolve some of these questions with regard to the different therapeutic properties of ACE inhibitors and ARBs. Until the results of this trial are available, there is space for individual weighting of data and personal opinions, which is nicely expressed by this discussion.

We declare that we have no conflict of interest other than that stated in the original paper.

*R E Schmieder, K F Hilgers, M P Schlaich MP, B M Schmidt
roland.schmieder@rzmail.uni-erlangen.de

Department of Nephrology and Hypertension, University of Erlangen-Nuremberg, 91054 Erlangen, Germany

1 Dickstein K, Kjekshus J; OPTIMAAL Steering Committee of the OPTIMAAL Study Group. Effects of losartan and captopril on mortality and morbidity in high-risk patients after acute myocardial infarction: the OPTIMAAL randomised trial. *Lancet* 2002; **360**: 752–60.
2 Pfeffer MA, McMurray JJ, Velazquez EJ, et al; Valsartan in Acute Myocardial Infarction Trial Investigators. Valsartan, captopril, or both in myocardial infarction complicated by heart failure, left ventricular dysfunction, or both. *N Engl J Med* 2003; **349**: 1893–906.
3 Demers C, McMurray JJ, Swedberg K, et al; CHARM Investigators. Impact of candesartan on nonfatal myocardial infarction and cardiovascular death in patients with heart failure. *JAMA* 2005; **294**: 1794–98.
4 Pourdjabbar A, Lapointe N, Rouleau JL. Angiotensin receptor blockers: powerful evidence with cardiovascular outcomes? *Can J Cardiol* 2002; **18** (suppl A): 7A–14A.

Prevention of postextubation laryngeal oedema

Bruno François and colleagues (March 31, p 1083)[1] describe a simple and safe intervention that could decrease the incidence of postextubation laryngeal oedema in critically ill patients. However, before recommending routine steroid treatment, more information is needed.

First, a more detailed description of the study population would help clinicians determine if the groups were balanced and whether extrapolation to other intensive-care units is warranted. In particular, it would be useful to know how many patients had signs and symptoms associated with reintubation,[2] such as depressed mental status, excess secretions, and weak cough.[3] Each of these could present with upper airway findings and be confused with laryngeal oedema, particularly if laryngoscopy is not done.

Second, François and colleagues should reconcile "planned extubation" with current practice. Standard recommendations do not include advanced planning for extubation but, rather, encourage clinicians to test candidates for extubation with daily spontaneous breathing trials.[4] Patients who prove to be capable of spontaneous breathing are considered for prompt extubation. This practice does not include a 12-h delay for steroids to take effect. Even if steroids were given in advance of the trials, how clinicians could reliably identify patients who will prove incapable of spontaneous breathing is unclear; for such patients, steroids would be inappropriate.

The move to "routine use of this treatment", as suggested in the accompanying Comment by Rupert Pearse and Duncan Young,[5] must be considered premature, pending answers to these questions.

I declare that I have no conflict of interest.

Mark D Siegel
Mark.Siegel@yale.edu

Yale University School of Medicine, 333 Cedar Street, New Haven, CT 06510, USA

1 François B, Bellissant E, Gissot V, et al. 12-h pretreatment with methylprednisolone versus placebo for prevention of postextubation laryngeal oedema: a randomised double-blind trial. *Lancet* 2007; **369**: 1083–89.
2 Epstein SK, Ciubotaru RL. Independent effects of etiology of failure and time to reintubation on outcome for patients failing extubation. *Am J Respir Crit Care Med* 1998; **158**: 489–93.
3 Salam A, Tilluckdharry L, Amoateng-Adjepong Y, Manthous CA. Neurologic status, cough, secretions and extubation outcomes. *Intensive Care Med* 2004; **30**: 1334–39.
4 McIntyre NR. Evidence-based guidelines for weaning and discontinuing ventilatory support. *Chest* 2001; **120**: 375S–96S.
5 Pearse RM, Young JD. Steroids to prevent postextubation laryngeal oedema. *Lancet* 2007; **369**: 1060–61.

In their useful study, Bruno François and colleagues[1] report successful treatment with methylprednisolone for the prevention of postextubation laryngeal oedema.

However, since severe oedema requiring reintubation is rare but potentially fatal, the proportion of patients excluded in this study (1727 of 2488 patients) is a concern. In particular, whether the duration of intubation is a risk factor for oedema remains controversial,[2,3] and the number of patients who were excluded from this study but who might have benefited from the use of corticosteroids before extubation could be significant.

Although screening for postextubation laryngeal oedema by use of the cuff-leak test is not a sufficient test because of the low positive predictive value, its high negative predictive value and low rate of complications suggest that this test might have been used to identify high-risk patients among the population excluded from this study.[2]

The incidence of adverse events in this population is also informative.

We declare that we have no conflict of interest.

Yasushi Goto, Takahide Nagase
ygoto-tky@umin.net

Department of Respiratory Medicine, University of Tokyo, Graduate School of Medicine, Hongo 7-3-1, Bunkyo-ku, Tokyo 113-8655, Japan

1 François B, Bellissant E, Gissot V, et al. 12-h pretreatment with methylprednisolone versus placebo for prevention of postextubation laryngeal oedema: a randomised double-blind trial. *Lancet* 2007; **369**: 1083–89.
2 Chung YH, Chao TY, Chiu CT, Lin MC. The cuff-leak test is a simple tool to verify severe laryngeal edema in patients undergoing long-term mechanical ventilation. *Crit Care Med* 2006; **34**: 409–14.
3 Stauffer JL, Olson DE, Petty TL. Complications and consequences of endotracheal intubation and tracheotomy: a prospective study of 150 critically ill adult patients. *Am J Med* 1981; **70**: 65–76.


Science Photo Library

I commend Bruno François and colleagues[1] for having successfully completed their challenging clinical trial of methylprednisolone to prevent postextubation laryngeal oedema.

Although I found the primary efficacy data compelling, I am left

ARTICLE

Homozygosity Haplotype Allows a Genomewide Search for the Autosomal Segments Shared among Patients

Hitoshi Miyazawa,* Masaaki Kato,* Takuya Awata, Masakazu Kohda, Hiroyasu Iwasa, Nobuyuki Koyama, Tomoaki Tanaka, Huqun, Shunei Kyo, Yasushi Okazaki, and Koichi Hagiwara

A promising strategy for identifying disease susceptibility genes for both single- and multiple-gene diseases is to search patients' autosomes for shared chromosomal segments derived from a common ancestor. Such segments are characterized by the distinct identity of their haplotype. The methods and algorithms currently available have only a limited capability for determining a high-resolution haplotype genomewide. We herein introduce the homozygosity haplotype (HH), a haplotype described by the homozygous SNPs that are easily obtained from high-density SNP genotyping data. The HH represents haplotypes of both copies of homologous autosomes, allowing for direct comparisons of the autosomes among multiple patients and enabling the identification of the shared segments. The HH successfully detected the shared segments from members of a large family with Marfan syndrome, which is an autosomal dominant, single-gene disease. It also detected the shared segments from patients with model multigene diseases originating with common ancestors who lived 10–25 generations ago. The HH is therefore considered to be useful for the identification of disease susceptibility genes in both single- and multiple-gene diseases.

Current genetic approaches focus on the identification of disease susceptibility genes (hereafter referred to as "disease genes") by exploiting the cosegregation of the disease phenotype over generations with a disease gene as well as a set of polymorphic marker types in its neighborhood (i.e., the haplotype). In a large family including multiple patients with a specific disease, the disease gene is usually derived from a single ancestor. On the basis of this assumption, haplotype analysis[1] or linkage analysis[2] has been used to find the gene. In affected-sib-pair analysis, a sib pair affected with the same disease is considered to share the same disease gene, inherited from their parents. The gene is searched for by looking at the genetic markers shared by the pair.[1,3] In whole-genome association studies, researchers try to capture segments containing disease-risk alleles derived from a limited number of very ancient ancestors where a haplotype block is the ultimate unit of search.[4–6] Because the haplotype contains the canonical information for every approach, determination of the haplotype is considered to greatly simplify the analyses.[7] However, the haplotype is not easy to identify in diploid organisms such as humans, because the genotypes of polymorphic markers are obtained as a mixture of those of the two alleles. Although many methods have been developed to reconstruct the haplotype,[1,7–9] their capabilities are limited. It is currently not possible, at least on a genomewide basis, to obtain haplotype information from an arbitrary subject or to compare two unrelated subjects in order to search for chromosomal segments sharing the same haplotype. In this study, we introduce the homozygosity haplotype (HH), which overcomes a part of this problem. The HH is a form of haplotype described by the homozygous SNPs, and, therefore, it is easily obtained genomewide. Using a family affected with Marfan syndrome (MIM 154700) and patients with model multigene diseases, we demonstrate how HH analysis allows the identification of the location of disease genes.

Material and Methods

Definition of Terms

Homozygosity haplotype (HH).—An HH is a haplotype described by only homozygous SNPs and is obtained by the deletion of heterozygous SNPs (fig. 1*Ai*), leaving only the homozygous SNPs (fig. 1*Aii*). At this point, the haplotype of each chromosome is uniquely determined, because all SNPs are homozygous (fig. 1*Aiii*). Note that both copies of homologous autosomes have the same HH over their entire length.

Comparable SNP (compSNP).—A compSNP is a SNP that is homozygous in two subjects (fig. 1*B*). We can compare the HHs between two subjects by use of the compSNPs (fig. 1*C*).

Region with a conserved HH (RCHH).—An RCHH is a run of compSNPs matched for allelic type, the genetic length of which is longer than the cutoff value (fig. 1*C*). An RCHH is bounded by either a mismatched compSNP(s) or by the end(s) of an autosome. The RCHHs shared by multiple subjects are the overlap of the RCHHs for each subject pair (fig. 1*D*).

Region from a common ancestor (RCA).—An RCA is an autosomal

Department of Respiratory Medicine (H.M.; N.K.; T.T.; H.; K.H.), Department of Cardiovascular Surgery (M. Kato; S.K.), Division of Endocrinology and Diabetes, Department of Medicine (T.A.), Division of Radioisotope Laboratory, Biomedical Research Center (T.A.), Division of Functional Genomics and Systems Medicine, Research Center for Genomic Medicine (M. Kohda; H.I.; Y.O.), and Division of Translational Research, Research Center for Genomic Medicine (M. Kohda; H.I.; Y.O.), Saitama Medical University

Received January 23, 2007; accepted for publication March 16, 2007; electronically published May 2, 2007.

Address for correspondence and reprints: Prof. Koichi Hagiwara, Department of Respiratory Medicine, Saitama Medical University, 38 Morohongo, Moroyama-machi, Saitama 350-0495, Japan. E-mail: hagiwark@saitama-med.ac.jp

* These two authors contributed equally to this work.

Am. J. Hum. Genet. 2007;80:1090–1102. 0002-9297/2007/8006-0009$15.00
DOI: 10.1086/518176

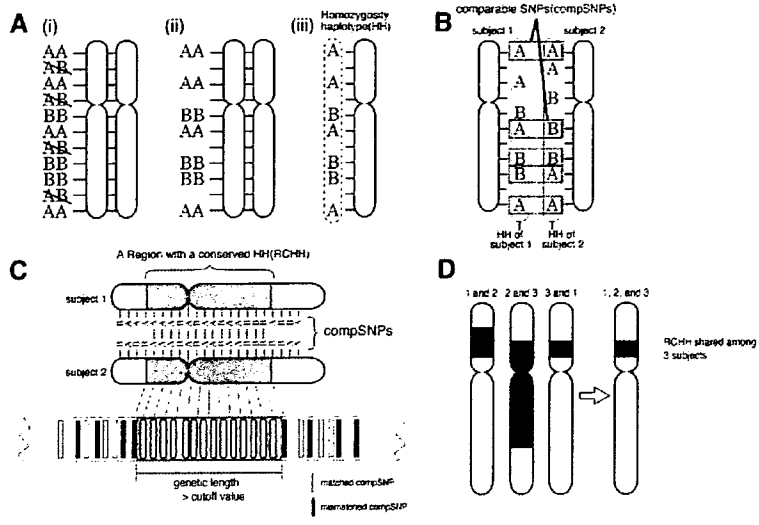

Figure 1. HH analysis. *A*, "A" denotes the major allelic type for each SNP. "B" denotes the minor allelic type for each SNP. *B*, Definition of a compSNP. *C*, Definition of an RCHH. An RCHH has a genetic length longer than the cutoff value. *D*, The definitions of an RCHH shared among multiple patients.

region where subjects share a chromosomal segment derived from a common ancestor (i.e., a segment identical by descent) (fig. 2*A*). In an RCA, subjects share the same segment on one or both copies of their homologous autosomes and thus share the same HH. Conversely, when subjects have the HH in a region, it suggests the presence of an RCA. Note that the RCA is unknown, and its presence is merely predicted through the RCHHs (see the section entitled "The RCHHs, False Negatives, Type A False Positives, and Type B False Positives").

The average genetic length of the RCAs decreases over generations. Figure 2*B* is a model pedigree with common ancestors (A and B). Two descendants (M and N), who are m and n generations removed from their common ancestors, share the RCAs derived from A and B. Assuming that the spouses (shown in gray shapes in fig. 2*B*) are not the descendants of A or B, then RCA(m,n) is the ratio of the total genetic length of the A- or B-derived RCA to the entire length of the autosomes. It is expressed as

$$\mathrm{RCA}(m,n{:}m \geq n) = \begin{cases} 2^{-m+1} & m \geq 1, n = 0 \\ \dfrac{3}{4} & m = 1, n = 1 \\ 2^{-m-n+2} & \text{otherwise.} \end{cases} \qquad (1)$$

A detailed description of the deduction of equation (1) is given in appendix A. Note that RCA(1,0) is equal to 1, indicating that a parent and a child (i.e., $m = 1$, $n = 0$) share the RCAs over the entire lengths of their autosomes.

Crossover Model and Data Analysis

We used the Haldane's Poisson process model[10] for the occurrence of crossovers and performed all calculations on the basis of this model. Information on SNPs used by the 500K GeneChips Mapping Array Set (Affymetrix) was summarized in the GeneChip annotation files (4/13/2006 version; see Affymetrix Web site), where, for each SNP, the genetic distance from the telomere of the short arm of the chromosome was obtained by interpolation from the sex-averaged data by deCODE Genetics.[11] The genetic length of an RCHH is the genetic distance between its bounding compSNPs.

We restricted our analysis to a total of 492,554 SNPs that had assigned dbSNP refIDs (see National Center for Biology Information Web site). The computer programs were written in the C programming language and were compiled by the GNU C compiler 4.0 (see the GNU Compiler Collection Web site). The program is available from our Web site and from the Saitama Medical University Web site.

The RCHHs, False Negatives, Type A False Positives, and Type B False Positives

When subjects who have common ancestors suffer from the same disease, the RCAs are the candidate regions in which to look for the disease gene. Because many RCAs are contained in the RCHHs, we established an algorithm that detects the RCHHs, thereby allowing us to identify the disease gene. As described, an RCHH is defined when a run of type-matched compSNPs is longer than the cutoff value (fig. 3*A*). Many RCHHs contain the RCAs; however, some do not. We defined three types of errors (fig. 3*B*). The false negatives are the RCAs that are not contained in the RCHHs. The type A false positives are the RCHHs that do not contain the RCAs. The type B false positives are the spaces between a containing RCHH and a contained RCA. The equations to calculate each of these errors are given in appendix A. Before the analysis, we calculated the ratios of the false negatives to the total length of the RCAs and of the type A and type B false positives to the entire length of the autosomes for a range of cutoff values, and we selected a value that minimizes the influence of errors.

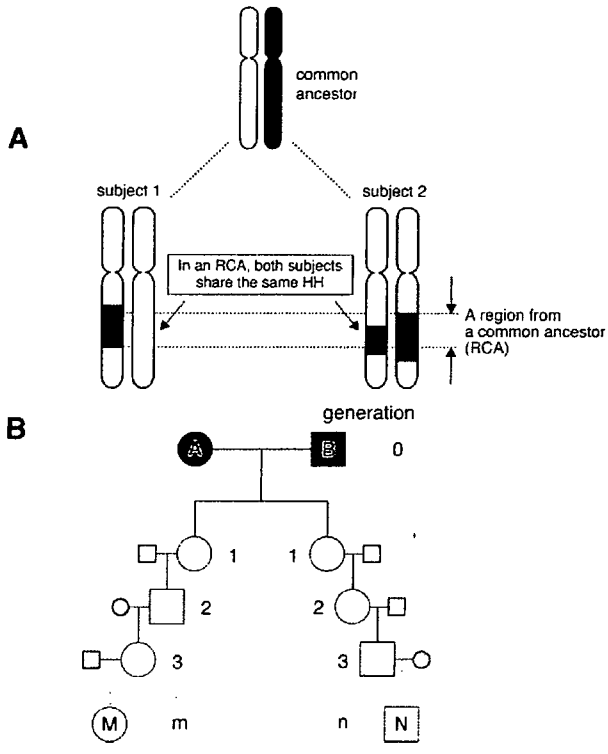

Figure 2. The RCA. *A*, The definition of an RCA. Gray regions are those derived from a single ancestral autosome from a single ancestor (segments identical by descent). A subject may have two copies of the segments in case inbreeding exists. *B*, A model pedigree. "A" and "B" denote the common ancestors. M and N are *m* and *n* generations away from the common ancestors. Direct offspring are shown by unfilled shapes. The spouse of each offspring is shown as a gray shape.

Human Subjects

This study was approved by the institutional review board of Saitama Medical University. All DNA samples were purified from peripheral blood drawn after written informed consent had been obtained. A family that included multiple patients with Marfan syndrome was genotyped, as were 46 unrelated subjects. In addition, the genotyping data from 45 unrelated Japanese subjects who had been enrolled in the International HapMap project (see International HapMap Web site) were obtained from the Affymetrix Web site (an average of 199,400 SNPs per subject had confidence values <.05).

Genotyping

Genomewide SNP genotypings were performed using the 500K GeneChips Mapping Array Set (i.e., the GeneChip Human Mapping 250K Nsp Array plus the GeneChip Human Mapping 250K Sty Array) (Affymetrix) or either of the two arrays. (Hereafter, the 500K GeneChips Mapping Array Sets will be abbreviated as "500k GeneChips" and the GeneChip Human Mapping 250K Nsp Array as "250k GeneChips.") 500k GeneChips was used for the analysis of the family with Marfan syndrome. 250k GeneChips was used for the multigene disease simulation.

Pools of Subjects

In the multigene disease simulations, genotyping data of patients who share an RCA at a specific position were constructed by replacing that part of their genotyping data with the genotyping data of a specific subject who acts as a common ancestor. The length of the replaced segment (x, in centimorgans) was taken at random from an exponential distribution with a probability density function of

$$f(x) = \lambda e^{-\lambda x} ,$$

$$\lambda = \frac{m}{100} , \qquad (2)$$

where m is the age, in generations, of the common ancestor.

Statistical Analysis

The numbers of subjects who share an RCHH at a given position on an autosome were compared between the patient pool and the control pool. The assumption was made that

$$u_0 = \frac{\hat{P}_1^* - \hat{P}_2^*}{\sqrt{\hat{P}^*(1-\hat{P}^*)\left(\frac{1}{n_1}+\frac{1}{n_2}\right)}}$$

has a standard normal distribution, where $\hat{P}_1^* = \frac{x_1+0.5}{n_1+1}$, $\hat{P}_2^* = \frac{x_2+0.5}{n_2+1}$, $\hat{P}^* = \frac{x_1+x_2+0.5}{n_1+n_2+1}$, x_1, and x_2 are the numbers of subjects sharing RCHHs in the patient pool and the control pool, respectively, and n_1 and n_2 are the total numbers of subjects in the patient pool and the control pool, respectively. The P value was calculated by

$$P = \int_{u_0}^{\infty} \frac{1}{\sqrt{2\pi}} e^{-\frac{x^2}{2}} dx .$$

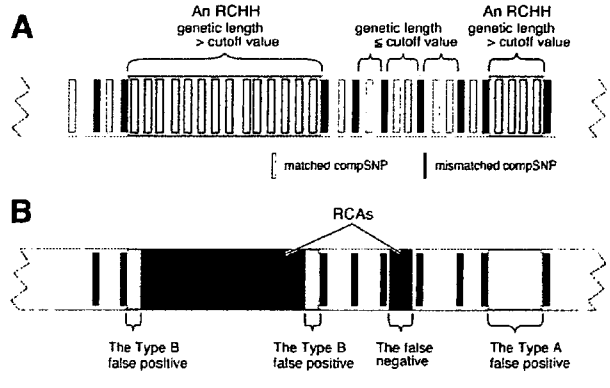

Figure 3. RCHHs, false negatives, type A false positives, and type B false positives. *A*, Detection of an RCHH. An RCHH has a genetic length longer than the cutoff value. *B*, Relationship of an RCHH and an RCA. The RCAs are overlaid and shown by dark gray boxes, and the RCHHs are shown by light gray boxes. Three types of errors are defined.

Results

Analysis of a Family with Marfan Syndrome

To investigate the utility of the HH in a family analysis, we studied a family that has multiple patients with Marfan syndrome. Marfan syndrome is an autosomal dominant disease characterized by an abnormality in the connective tissue. Mutations of either the fibrillin-1 gene (*FBN-1*) on 15q21.1 or of the TGF-β type II receptor gene (*TGFBR2*) on 3p24.2 are known to be the cause of this syndrome.[12] The family had been studied, and six symptomatic members and three asymptomatic carriers had a heterozygous 1879C→T (R627C) mutation in *FBN-1* (fig. 4*A*). Subject I-1 is considered to be the common ancestor for the disease gene. The questions we posed were as follows: (i) Could the HH identify the region containing *FBN-1* by the data from six symptomatic members? and (ii) Could the HH further narrow the region with the inclusion into the analysis of three asymptomatic carriers?

Before beginning our analysis, we checked the accuracy of the genotyping data. Equation (1) indicates that a parent and a child share the same HH along the entire length of their autosomes. Therefore, the ratio of the number of the matched compSNPs to the total number of compSNPs indicates the accuracy of genotyping. We studied three pairs: II-1 and III-4, II-3 and III-1, and II-5 and III-3. In a GeneChip analysis, the genotyping result for each SNP is

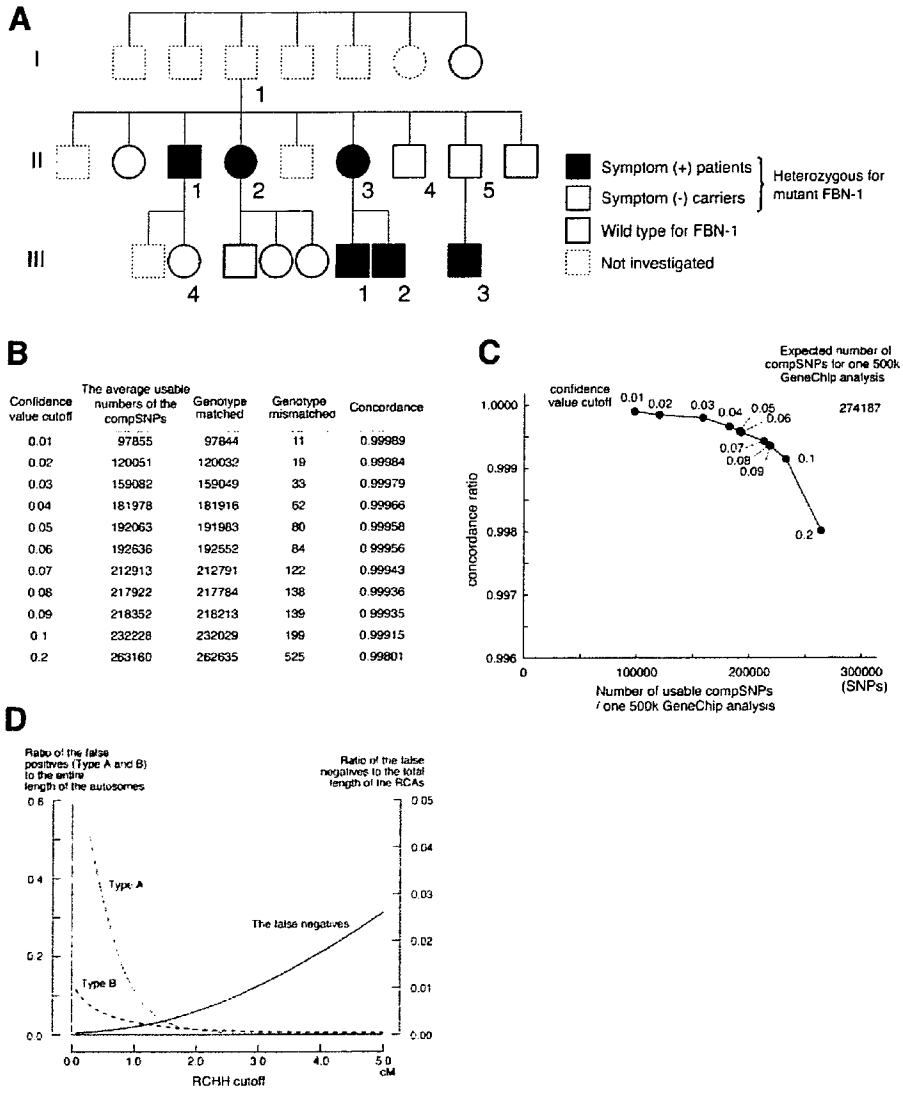

Figure 4. Accuracy of the GeneChip data. *A*, Pedigree of a family with Marfan syndrome. *B*, Relationship between the confidence-value cutoffs and the concordance ratios. *C*, Schematic presentation of the data in panel B. *D*, False negatives between two subjects in generation III and the average ratio of the type A false positives and the type B false positives to the entire length of the autosomes for all combinations of subjects were plotted for a range of RCHH cutoffs.

accompanied by a confidence value; the smaller the confidence values, the more reliable the data. The concordance ratios of the compSNPs in three parent-child pairs for a range of confidence-value cutoffs are shown in figure 4*B* and 4*C*. We chose a confidence-value cutoff of .05.

Secondly, we determined the cutoff value for defining the RCHHs (hereafter, an "RCHH cutoff"). Figure 4*D* shows the relationship of the RCHH cutoffs and three types of errors. We chose 3.0 cM because it gave small rates of type A and type B false positives with an acceptable value for the false negatives.

We then analyzed six symptomatic patients. In figure 5, we present the result stepwise. Patients II-3 and III-1 are a parent-child pair who share RCHHs over the entire length of the autosomes (fig. 5*A*). II-1 and II-2 are siblings whose RCHHs occupy 81% of the autosomes (eq. [1] predicted 75%) (fig. 5*B*). II-2 and III-1 are an aunt and nephew whose RCHHs occupy 56% of the autosomes (eq. [1] predicted 50%) (fig. 5*C*). III-2 and III-3 are first cousins whose RCHHs occupy 39% of the autosomes (eq. [1] predicted 25%) (fig. 5*D*). The RCHHs conserved among all symptomatic members contained 96% of the total length of the RCA (calculated from table A1), and they did indeed contain *FBN-1* (fig. 5*E*). The inclusion of asymptomatic carriers (II-4, II-5, and III-4) (see fig. 4*A*) did further narrow the RCHHs (fig. 5*F*). These results demonstrate that HH analysis is both efficient and intuitive for identifying the location of disease genes in a large family.

Simulation of a Multigene Disease

Each multigene disease has a specific genetic structure. Some are considered to be a collection of single-gene diseases of which the phenotypes are indistinguishable from each other. In others, several genes working together are required to produce symptoms.[13] In either case, a subgroup of patients may share a disease gene from a common ancestor.

To investigate the utility of the HH in multigene diseases, we investigated a model multigene disease (fig. 6*A*). Here, SNP *rs16823424* (the 100,000th SNP on 500k GeneChip) is the location of the disease gene. In this region, 15 patients share an RCA derived from a common ancestor who lived 10 generations ago. The genotyping data around *rs16823424* in these 15 patients were replaced with the genotyping data at the corresponding position from a specific person who, in this analysis, acts as the common ancestor (fig. 6*B*). The lengths of the replacements were taken at random from an exponential distribution (eq. [2]: $m = 10$). Therefore, comparison of two patients corresponds with the situation $m = n = 10$ in fig. 2*B*. The patient pool included these 15 subjects together with 30 unrelated subjects (fig. 6*C*). The control pool consists of 45 unrelated Japanese samples obtained from the Affymetrix Web site. Our aim was to identify the *rs16823424* region. The strategy was as follows. In step 1, we divided autosomal regions into minute regions. In step 2, using the patient pool, we identified the HH shared by the greatest number of subjects for each region (i.e., the most common HH). We then concatenated the most common HHs for each region into a virtual HH for the entire autosome. A virtual subject who has this virtual HH was named "the representative" (step 1 in fig. 6*C*). The subjects were counted who shared the RCHHs with "the representative" in both the patient pool and the control pool for each region (step 2 in fig. 6*C*). Finally, the differences between the pools were expressed by *P* values. The candidate region for the disease gene is the region that has the lowest *P* value (i.e., the greatest $-\log_{10}(P)$ value) in the entire autosome.

Before the analysis, we determined an appropriate RCHH cutoff (fig. 6*D*). Here, the false negatives were plotted for several ages of common ancestors (the ages are expressed by m and n). As the number of generations increases, the length of the RCA shortens, increasing the difficulty of its detection with increasingly high m and n values. Because an RCHH cutoff of 5 cM was considered suitable for $m = n = 10$, this value is used hereafter. The false negatives to the total length of the RCAs decreases as we include more SNPs in the analysis. This will be discussed later.

We then performed the analysis. Figure 6*E* is a densitogram of the $-\log_{10}(P)$ value; the denser the areas are, the higher the significance. The *rs16823424* region provided a $-\log_{10}(P)$ of 4.48, and was the only region with a $-\log_{10}(P) > 3.0$ (i.e., $P < .001$). The greatest $-\log_{10}(P)$ outside of the *rs16823424* region was 2.92, which provides the background of the analysis.

Next, we investigated the detection limit. For each number from 7 to 15, we constructed 100 patient pools in which that number of patients, out of 45, shared an RCA at the *rs16823424* region. When the number is <9, the background value overwhelmed the signal in most of the analyses (fig. 6*F*). Therefore, 10 of 45 patients (22%) was the detection limit of this analysis.

Detection of Multiple Targets and the Effect of Age of Common Ancestors

We next simulated a multigene disease with three different causative genes: one at *rs16823424* (the 100,000th SNP on 500k GeneChips), one at *rs4473885* (the 200,000th SNP), and one at *rs11200928* (the 300,000th SNP). The ages of the common ancestors were $m = n = 15$, 20, and 25. We generated 100 sets of 45 subjects. Subjects 1–15 had a segment replaced with that of a specific person (the common ancestor) for a length taken at random from an exponential distribution corresponding to $m = n = 15$. Subjects 16–30 had a segment replaced corresponding to $m = n = 20$. Subjects 31–45 had a segment replaced corresponding to $m = n = 25$ (fig. 7*A*). The analysis was performed with an RCHH cutoff of 5.0 cM. Figure 7*B* demonstrates the detection of three targets simultaneously. The detection limits were 10 (22%) ($m = n = 15$), 13

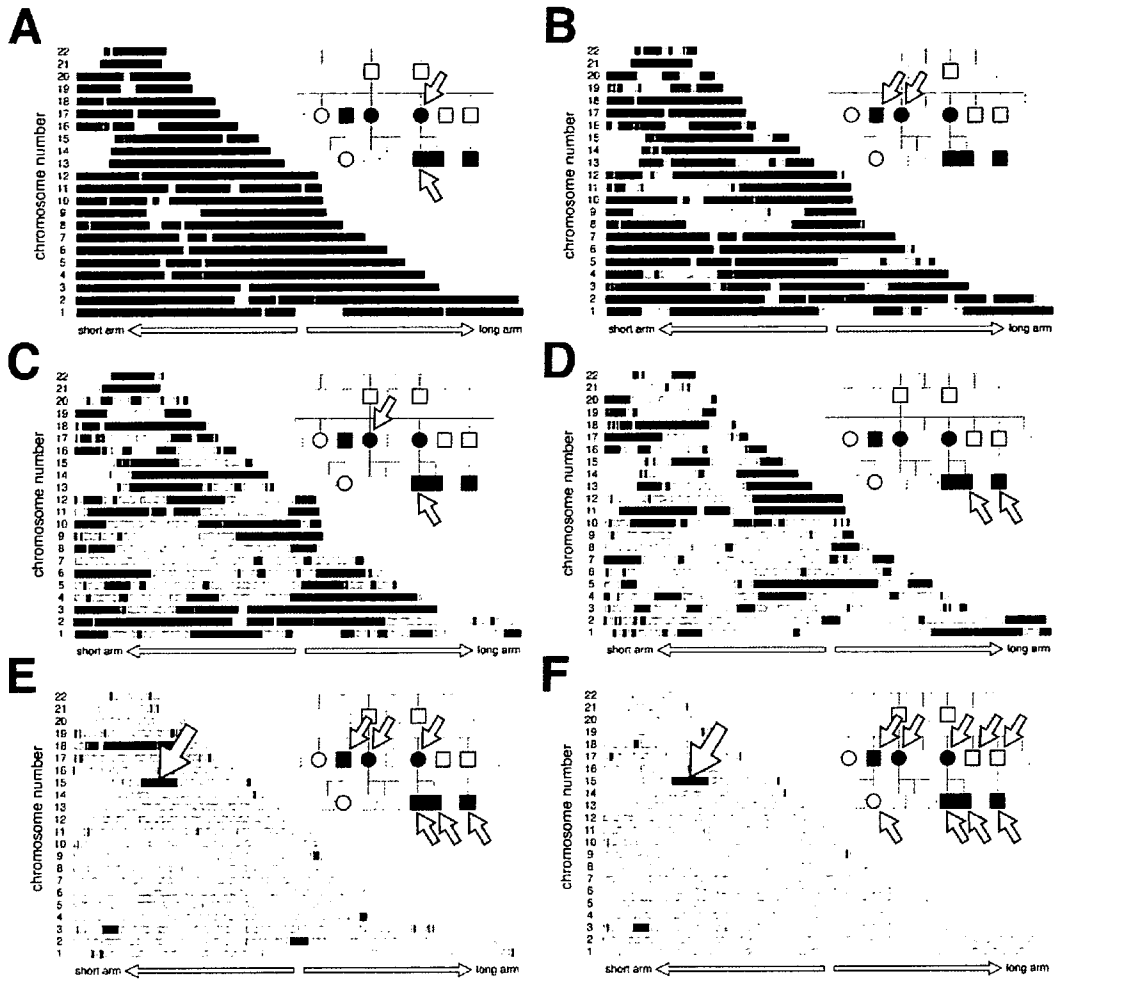

Figure 5. Family analysis. Identification of the candidate regions for the disease gene for a family with Marfan syndrome. The RCHHs are shown in black, whereas the other autosomal regions are shown in gray. *A*, The RCHHs between a parent and child, indicated by arrows, are shown. *B*, The RCHHs between siblings. *C*, The RCHHs between an aunt and nephew. *D*, The RCHHs between first cousins. *E*, The RCHHs for all symptomatic members. The *FBN-1* gene is located in the RCHH (19.6 cM in length) indicated by a large arrow. *F*, The RCHHs for all nine members (six symptomatic members and three asymptomatic carriers) who have a mutation in the *FBN-1* gene.

(29%) ($m = n = 20$) and 13 (29%) ($m = n = 25$) of 45 patients.

Discussion

In this study, we introduce HH analysis. Both copies of the homologous autosomes have the same HH and thus can be handled as if they were a single chromosome with a single HH. This enables the direct comparison of the autosomes between two individuals and thereby enables a search for a shared ancestral segment.

Because HH analysis looks for the ancestral segments, both dominant and recessive genes can be detected. The analysis is nonparametric—that is, it does not require the information from the pedigree. The patient pool contains only affected subjects, and therefore information on penetrance is not necessary. All these characteristics make the design and the interpretation of analyses simple.

Another characteristic of HH analysis is the simplicity of the algorithm, and therefore the calculation may be performed on many personal computers. The calculation for a family with Marfan syndrome that contains nine subjects (fig. 5) is completed in 6 s on our laptop computer. The analysis composed of two pools containing 45 subjects each (fig. 6*E*) took 5 min. The calculation time is proportional to the square of the number of subjects, and thus analyses with a larger number of subjects are not difficult to perform.

We used the classical Haldane's Poisson model for the calculations. In an actual situation, the crossovers do not occur randomly along the length of the autosomes. One of the major causes of the deviation from the model is

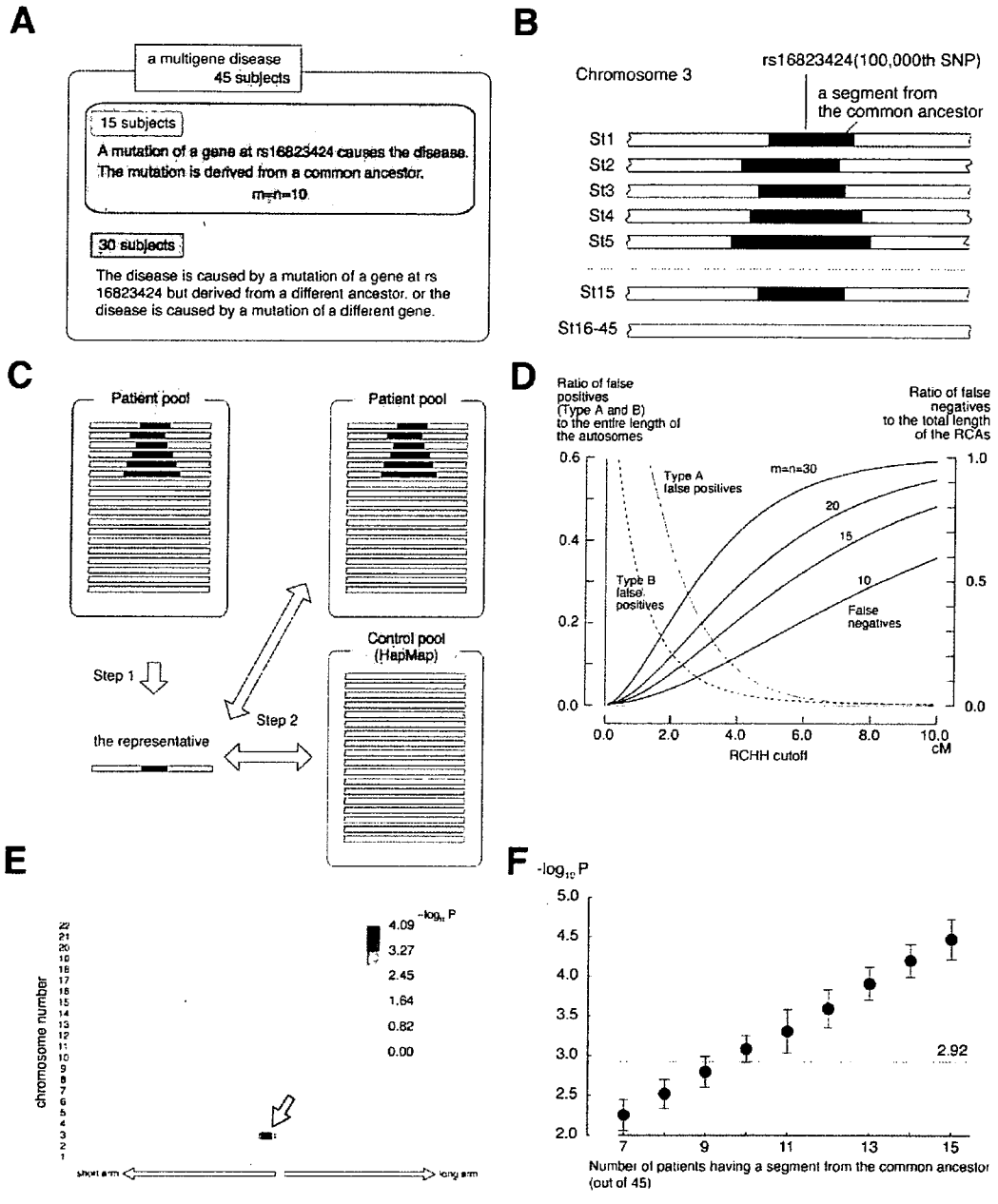

Figure 6. Simulation of a multigene disease. *A,* The structure of a model multigene disease. In 15 patients, a causative mutation of the gene at *rs16823424* is derived from a common ancestor. In the remaining 30 patients, the mutation may be from a different ancestor, or the mutations may occur in a different disease gene(s). *B,* Construction of a patient pool. Black bars indicate segments at the *rs16823424* region taken from the common ancestor. St = subject. *C,* Analysis procedure. *D,* The average ratios of the type A false positives and the type B false positives to the entire length of the autosomes for all combinations of the subjects in the control pool. The ratio of the false negatives to the total length of the RCAs for several values of *m* and *n* are simultaneously shown. *E,* Densitogram of $-\log_{10}(P)$ value for each region of the autosomes. A region that is 2.92 cM in length and contains *rs16823424* (indicated by a white arrow) gave the greatest $-\log_{10}(P)$ value, 4.09. *F,* The distribution of $-\log_{10}(P)$ from the analyses using 100 patient pools for each number of patients is shown as mean ± SD. The highest background value is 2.92 (i.e., the greatest $-\log_{10}(P)$ value outside of the *rs16823424* region).